NeuroImage 187 (2019) 17–31

Contents lists available at ScienceDirect

NeuroImage

journal homepage: www.elsevier.com/locate/neuroimage

MRI techniques to measure arterial and venous cerebral blood volume

Jun Hua [a,b,*], Peiying Liu [a,b], Tae Kim [c,d], Manus Donahue [e,f], Swati Rane [g], J. Jean Chen [h,i], Qin Qin [a,b], Seong-Gi Kim [j,k]

[a] Neurosection, Div. of MRI Research, Dept. of Radiology, Johns Hopkins University School of Medicine, Baltimore, MD, USA
[b] F.M. Kirby Research Center for Functional Brain Imaging, Kennedy Krieger Institute, Baltimore, MD, USA
[c] Department of Radiology, University of Pittsburgh, Pittsburgh, PA, USA
[d] Department of Bioengineering, University of Pittsburgh, Pittsburgh, PA, USA
[e] Department of Radiology and Radiological Sciences, Vanderbilt University Medical Center, Nashville, TN, USA
[f] Department of Neurology, Vanderbilt University Medical Center, Nashville, TN, USA
[g] Radiology, University of Washington Medical Center, Seattle, WA, USA
[h] Rotman Research Institute, Baycrest Centre, Canada
[i] Department of Medical Biophysics, University of Toronto, Canada
[j] Center for Neuroscience Imaging Research, Institute for Basic Science (IBS), Suwon, South Korea
[k] Department of Biomedical Engineering, Sungkyunkwan University, Suwon, South Korea

ARTICLE INFO

Keywords:
MRI
CBV
Pial artery
Arteriole
Capillary
Venule
Vein

ABSTRACT

The measurement of cerebral blood volume (CBV) has been the topic of numerous neuroimaging studies. To date, however, most *in vivo* imaging approaches can only measure CBV summed over all types of blood vessels, including arterial, capillary and venous vessels in the microvasculature (i.e. total CBV or CBVtot). As different types of blood vessels have intrinsically different anatomy, function and physiology, the ability to quantify CBV in different segments of the microvascular tree may furnish information that is not obtainable from CBVtot, and may provide a more sensitive and specific measure for the underlying physiology. This review attempts to summarize major efforts in the development of MRI techniques to measure arterial (CBVa) and venous CBV (CBVv) separately. Advantages and disadvantages of each type of method are discussed. Applications of some of the methods in the investigation of flow-volume coupling in healthy brains, and in the detection of pathophysiological abnormalities in brain diseases such as arterial steno-occlusive disease, brain tumors, schizophrenia, Huntington's disease, Alzheimer's disease, and hypertension are demonstrated. We believe that the continual development of MRI approaches for the measurement of compartment-specific CBV will likely provide essential imaging tools for the advancement and refinement of our knowledge on the exquisite details of the microvasculature in healthy and diseased brains.

Introduction

Cerebral blood volume (CBV) is an important physiological parameter reflecting the amount of blood in brain tissue (ml blood/100 ml tissue). Under normal physiological conditions, the brain attempts to maintain adequate cerebral blood flow (CBF, in units of ml blood/100 g tissue/minute) by regulating the caliber of arteries and arterioles through an auto-regulatory mechanism (Kuschinsky et al., 1996; Mchedlishvili, 1986). Thus, in early stages of cerebrovascular alterations, CBV can serve as a sensitive indicator for evaluating tissue viability and function. Baseline CBV also demonstrates strong correlations with basal metabolism in the brain (Gonzalez et al., 1995; Raichle, 1983). In addition, CBV is a major modulator of the blood-oxygen-level-dependent (BOLD) effect (Buxton and Frank, 1997; Ogawa et al., 1993; van Zijl et al., 1998), and thus has relevance for the interpretation of such BOLD functional MRI (fMRI) signals.

Various neuroimaging techniques have been developed to measure CBV. A common requirement of these approaches is the utilization of an endogenous or exogenous tracer to separate signal from the intravascular and extravascular compartments so that CBV (intravascular space) can be quantified (Kety and Schmidt, 1948). For instance, iodinated contrast agents are commonly used in computed tomography (CT) for measuring

* Corresponding author. Johns Hopkins University, School of Medicine, Department of Radiology, Kennedy Krieger Institute, F.M. Kirby Research Center for Functional Brain Imaging, 707 N Broadway, Baltimore, MD 21205, USA.
E-mail address: jhua@mri.jhu.edu (J. Hua).

https://doi.org/10.1016/j.neuroimage.2018.02.027
Received 15 November 2017; Received in revised form 12 February 2018; Accepted 14 February 2018
Available online 16 February 2018
1053-8119/

parenchymal perfusion parameters including CBV (Heit and Wintermark, 2016; Koenig et al., 1998). In positron emission tomography (PET), radioactive isotopes such as ^{15}O-labeled carbon monoxide (C^{15}O) (Grubb et al., 1974) are used to label the blood separately from extravascular tissue, so that CBV can be measured. More recently, several MRI techniques have been developed to measure CBV with intravascular paramagnetic and superparamagnetic contrast agents, such as Gd-DTPA (Belliveau et al., 1991; Lu et al., 2005; Moseley et al., 1992; Ostergaard et al., 1996a, 1996b; Uh et al., 2009) and ferumoxytol (D'Arceuil et al., 2013; Qiu et al., 2012) in humans, and MION (Leite et al., 2002; Mandeville et al., 1998) in animals; as well as blood water spins as intrinsic endogenous contrast sources such as in the vascular space occupancy (VASO) approach (Lu et al., 2003, 2013; Lu and van Zijl, 2012).

To date, most CBV imaging approaches measure total CBV (CBVtot), which reflects the sum of signals from the arterial, capillary and venous vessels in the microvasculature. However, different types of blood vessels have distinct functions and physiology, and can be affected differentially in brain diseases. The arterioles are actively regulated blood vessels, and thus may be more sensitive to metabolic disturbances in the brain (Iadecola and Nedergaard, 2007; Ito et al., 2001, 2005; Kim et al., 2007; Takano et al., 2006). During angiogenesis, some arterioles are generated before capillaries and before changes in CBF occur (Hansen-Smith et al., 2001). Recent evidence from animal models demonstrates that aging affects pial arteries and arterioles before capillaries and venous vessels, and that dysfunction in pial arteries occurs months before total CBF changes can be detected (Balbi et al., 2015). In early hypertensive-induced cerebrovascular alterations, CBV in arterial vessels is altered while CBF is still intact (Kim et al., 2014; Lee and Kim, 2017). On the other hand, venous blood vessels are less contractile, and venous blood flow is primarily influenced by the pressure and pulsation from arterial blood vessels (Schaller, 2004). The venous system is closely linked with the drainage of metabolic wastes from brain tissue and the interstitial and cerebrospinal fluids (Schaller, 2004), which has important clinical implications in many brain diseases (Iliff et al., 2012). For neuroimaging, blood oxygenation level changes during neuronal and physiological stimulation, which forms the physiological basis for the BOLD effect, primarily occur in venous vessels. Therefore, the measurement of CBV in each type of blood vessels separately may furnish information that is not obtainable from total CBV and CBF measures, and may provide a more sensitive and specific index for the underlying physiology in healthy and diseased brains.

The volume of arterial blood vessels (CBVa) is approximately 20–30% (Table 1) of the intravascular space occupied by all blood vessels (CBVtot), while the volume of venous blood vessels (CBVv, including capillaries) is approximately 70–80% (Table 2) of CBVtot at basal state in healthy brains (Piechnik et al., 2008; Sharan et al., 1989; van Zijl et al., 1998). Because of the smaller baseline fraction of CBVa/CBVtot compared to CBVv/CBVtot, it was often assumed that CBVa change in brain tissues during neuronal activity is negligible compared to CBVv and CBVtot changes (Buxton et al., 1998; Mandeville et al., 1998, 1999). However, recent imaging studies showed that during functional or physiological stimulation, CBVa can increase by up to 80% of its baseline values (Table 3). In contrast, the relative change in CBVv is usually much smaller than CBVa during functional stimulation (Table 4). Some studies even reported minimal changes in venule diameters (Hillman et al., 2007) and CBVv (Kim et al., 2007; Kim and Kim, 2010) during functional stimulation. Note that stimulus duration may be an important factor that affects CBVv change. Kim et al. found negligible CBVv change during a short (15 s) functional stimulus (Kim et al., 2007), but detected substantial CBVv increase during a long (40 s) functional stimulus (Kim and Kim, 2011). Similarly, CBVv increase or dilation of venules were found during a 96-s (Chen and Pike, 2009a) and a 240-s (Stefanovic and Pike, 2005) visual stimulation in humans, and during a 120-s direct electric stimulation in rats (Akgoren and Lauritzen, 1999). Such long stimuli typically induce initial fast CBVa increase followed by slow CBVv dilation, as demonstrated in fMRI experiments (Kim and Kim, 2011; Zong et al., 2012) and predicted in computational models of fluid dynamics (Barrett et al., 2012; Krieger et al., 2012). It should also be noted that CBVv changes during physiological challenges such as breathhold (Hua et al., 2010) or hypercapnia (Chen and Pike, 2010; Lee et al., 2001) are usually greater than those observed during functional (or neuronal) activation. Furthermore, blood vessels in different cortical layers (surface and deep layer vessels and penetrating arterioles and venules between layers) may have distinct responses to a given functional or physiological stimulation (Blinder et al., 2013; Huber et al., 2014; Tian et al., 2010), with important implications for high-resolution CBV based fMRI (Huber et al., 2017b).

In this review, we attempt to discuss recently developed MRI approaches for the measurement of CBV in arterial and venous blood vessels separately. CBV measured in physiological units (ml blood/100 ml tissue) is referred to as absolute CBV, whereas CBV difference between functional stimulation and baseline periods normalized by the baseline value is referred to as relative CBV change (%). We will also demonstrate how some of these methods have shown promising results to help us better understand vascular physiology in healthy brains and microvascular abnormalities in brain diseases. In this review, we will try to focus on the CBV imaging techniques that are specifically designed to distinguish arterial and venous CBV. For total CBV methods, the readers are referred to corresponding articles in this special issue and in the literature. Also, to keep this review concise, we will not show figures similar to the ones that have already been published in the referenced studies.

Table 1
CBVa values reported in the literature.

Reference	Species	Brain Region	Technique	CBVa (ml/100 ml)
(Neil and Ackerman, 1992)	Rat	Whole brain	MRI	1.00 ± 0.15
(Duong and Kim, 2000)	Rat	Whole brain	19F NMR	0.9 ± 0.2
(Lee et al., 2001)	Rat	Whole brain	19F NMR	0.78
(Ito et al., 2001)	Human	Cortex	PET	1.1 ± 0.4
(Barbier et al., 2001)	Rat	Cortex	MRI	0.82 ± 0.10
(An and Lin, 2002b)	Human	Whole brain	MRI	0.74 ± 0.20
(Ito et al., 2005)	Human	Cortex	PET	1.5 ± 0.3
(Kim and Kim, 2005, 2006)	Rat	Cortex	MRI	1.1 ± 0.5
		Caudate, Putamen		1.3 ± 0.6
(Petersen et al., 2006)	Human	Gray matter	MRI	0.93 ± 0.06
(Kim et al., 2007)	Rat	Somatosensory cortex	MRI	0.83 ± 0.21
(Brookes et al., 2007)	Human	Gray matter	MRI	1.7 ± 0.1
(Hendrikse et al., 2008)	Human	Anterior border zone	MRI	0.88 ± 0.07
		Posterior border zone		1.19 ± 0.11
		Non-border zone GM		1.64 ± 0.08
(Petersen et al., 2010)	Human	Gray matter	MRI	0.67 ± 0.16
(Hua et al., 2011b)	Human	Gray matter	MRI	0.76 ± 0.17
(Yan et al., 2012)	Human	Gray matter	MRI	1.14–2.05
		White matter		0.46–0.55
(Heijtel et al., 2016)	Human	Gray matter	MRI	0.84 ± 0.35
			PET	3.21 ± 0.45
		White matter	MRI	0.54 ± 0.26
			PET	1.87 ± 0.31
		Whole brain	MRI	0.70 ± 0.31
			PET	2.60 ± 0.38
(Kim et al., 2016)	Human	Gray matter	MRI	1.4–2.3
(Rane et al., 2016)	Human	Cortex	MRI	1.58–1.89
		Hippocampus		2.20–2.32

The percentage of CBVa/CBVtot depends on the CBVtot value used, which was estimated to be approximately 20–30% in (Piechnik et al., 2008; Sharan et al., 1989; van Zijl et al., 1998).

Table 2
CBVv values reported in the literature.

Reference	Species	Brain Region	Technique	CBVv (ml/100 ml)
(Ito et al., 2001)	Human	Cortex	PET	2.0 ± 0.2
(An and Lin, 2002a)	Human	Whole brain	MRI	2.68–2.97
(An and Lin, 2002b)	Human	Whole brain	MRI	2.46 ± 0.28
(An and Lin, 2003)	Human	Gray matter	MRI	4.0–5.5
		White matter		2.9–3.9
(Ito et al., 2005)	Human	Cortex	PET	1.9 ± 0.5
(Bulte et al., 2007a)	Huamn	Whole brain	MRI	3.77 ± 1.05
		Gray matter		3.93 ± 0.90
		White matter		2.52 ± 0.78
(He and Yablonskiy, 2007)	Human	Gray matter	MRI	1.75 ± 0.13
		White matter	MRI	0.58 ± 0.09
(He et al., 2008)	Rat	Whole brain	MRI	3.3 ± 0.5
(Sedlacik and Reichenbach, 2010)	Human	Gray matter	MRI	2.54 ± 0.40
		White matter		1.21 ± 0.35
(Blockley et al., 2013a)	Human	Gray matter	MRI	2.18 ± 0.41
		White matter		1.30 ± 0.24

CBVv measured by most MRI methods developed to date reflects the signals from vessels with partially deoxygenated blood, which may include contributions from capillaries, venules and veins.
The percentage of CBVv/CBVtot depends on the CBVtot value used, which was estimated to be approximately 70–80% in (Piechnik et al., 2008; Sharan et al., 1989; van Zijl et al., 1998).

Arterial cerebral blood volume (CBVa)

We define arterial blood vessels as pre-capillary vessels that can actively dilate or constrict to control cerebral perfusion and the delivery of oxygen and other nutrients to brain tissues. These include arteries, pial arteries and arterioles with a wide range of vessel diameters and blood flow velocities (Mchedlishvili, 1986). Immunohistochemistry studies show a layer of elastic lamina between the smooth muscle and the endothelial cells that is only present in cerebral arterioles, but not in cerebral venules and capillaries (Shen et al., 2012). In healthy brain parenchyma, CBVa is approximately 20–30% (Table 1) of CBVtot at baseline (Piechnik et al., 2008; Sharan et al., 1989; van Zijl et al., 1998). The relative change in CBVa (in percentage compared to baseline values) during functional stimulation is usually much greater than those in capillaries and venous vessels (Table 3), which is an important factor to consider when interpreting the BOLD signals (see section 4).

It is important to differentiate large arteries from smaller pial arteries and arterioles with diameters up to 100–150 μm, which is the primary regulator of local tissue perfusion (Auer and Johansson, 1980; Mchedlishvili, 1986; Mchedlishvili et al., 1974–75). Depending on the physical and/or physiological properties utilized to selectively label arterial blood, some approaches discussed below may be more sensitive to pial arteries and arterioles, whereas some may include substantial signal contributions from larger arteries as well. Here, we will discuss three main categories of MRI techniques for the measurement of CBVa *in vivo* based on the type of contrast used to differentiate arterial blood from the rest of the vasculature.

Approaches based on blood velocity

The velocity of blood flow in arterial vessels is usually much greater than that in capillaries and venous vessels. For instance, the average blood flow velocities in arterial vessels with diameters less than 50 μm, 50 to 100 μm, 100 to 150 μm, and 150 to 200 μm in cat brain were reported to be 1.29 ± 0.13, 2.46 ± 0.34, 4.21 ± 0.47, and 5.99 ± 0.53 (10^{-2} m/s), respectively (Kobari et al., 1984). On the other hand, blood flow velocities for capillaries (diameters < 20 μm) in the mouse brain and venules (diameters 20 to 60 μm) in the rat brain were reported to be 2.30 ± 0.58 (10^{-4} m/s) (Pan et al., 2014) and 0.57–1.52 (10^{-4} m/s) (Hillman et al., 2007), respectively. Although the reported values of blood flow velocities may vary depending on many factors, such as species, method of measurement and so on, the trend of faster flows in arterial vessels has been consistently observed (Piechnik et al., 2008).

In MRI, magnetic field gradients can be applied to dephase signals

Table 3
Relative CBVa changes during functional and physiological stimulation reported in the literature.

Reference	Species	Anesthesia	Stimulation		Technique	Relative CBVa change [a]
			Type	Duration		
(Iadecola et al., 1997)	Rat (cerebellum)	halothane	Electrical stimulation	20 s	Optical imaging	59%
(Lee et al., 2001)	Rat	α-chloralose	Hypercapnia	N/A	19F NMR, microscopy	79%
(Ito et al., 2005)	Human	N/A	Hypercapnia	N/A	PET	67%
(Takano et al., 2006)	Mouse (primary somatosensory cortex)	urethane and α-chloralose	Electrical stimulation	60 s	Optical imaging	39%
(Hillman et al., 2007)	Rat	α-chloralose	Forepaw stimulation	4 s	Optical imaging	37%
(Kim et al., 2007)	Rat	isoflurane	Forepaw stimulation	15 s	MRI	41%
(Brookes et al., 2007)	Human	N/A	Finger tapping	30 s	MRI	33%
(Francis et al., 2008)	Human	N/A	Visual	14 s	MRI	61%
(Kim et al., 2008)	Rat	isoflurane	Forepaw stimulation	15 s	MRI	46%
(Kim and Kim, 2010)	Cat	isoflurane	Visual	40 s	MRI	33%
(Kim and Kim, 2011)	Cat	isoflurane	Visual	40 s	MRI	24%
(Hua et al., 2011a)	Human	N/A	Visual	30 s	MRI	58%
(Hua et al., 2010; Hua et al., 2011c)	Human	N/A	Visual	15 s	MRI	54%
			Breathhold	15 s		53%
(Meng et al., 2012)	Rat	isoflurane	Forepaw stimulation	20 s	MRI	19%
		α-chloralose				46%
(Yan et al., 2012)	Human	N/A	Visual	67.5 s	MRI	50–67%
(Huber et al., 2014)	Human	N/A	Visual	30 s	MRI	55%
(Jahanian et al., 2015)	Human	N/A	Visual and sensorimotor	30 s	MRI	85%

[a] Relative CBVa change = 100 × (CBVa active – CBVa baseline)/(CBVa baseline) %.

Table 4
Relative CBVv changes during functional and physiological stimulation reported in the literature.

Reference	Species	Anesthesia	Stimulation		Technique	Relative CBVv change [a]
			Type	Duration		
(Lee et al., 2001)	Rat	α-chloralose	Hypercapnia	N/A	19F NMR, microscopy	11-23%
(An and Lin, 2003)	Human	N/A	Hypercapnia	N/A	MRI	14%
(Stefanovic and Pike, 2005)	Human	N/A	Visual	240 s	MRI	16%
(Ito et al., 2005)	Human	N/A	Hypercapnia	N/A	PET	0%
(Takano et al., 2006)	Mouse (primary somatosensory cortex)	urethane and α-chloralose	Electrical stimulation	60 s	Optical imaging	4%
(Hillman et al., 2007)	Rat	α-chloralose	Forepaw stimulation	4 s	Optical imaging	0%
(Kim et al., 2007)	Rat	isoflurane	Forepaw stimulation	15 s	MRI	0%
(Chen and Pike, 2009a)	Human	N/A	Visual and sensorimotor	96 s	MRI	9-14%
(Chen and Pike, 2009b)	Huamn	N/A	Visual and sensorimotor	24 s 96 s	MRI	Not reported 8-30%
(Chen and Pike, 2010)	Human	N/A	Hypercapnia	180 s	MRI	7-20%
(Kim and Kim, 2010)	Cat	isoflurane	Visual	40 s	MRI	2%
(Kim and Kim, 2011)	Cat	isoflurane	Visual	40 s	MRI	5%
(Hua et al., 2010; Hua et al., 2011c)	Human	N/A	Visual Breathhold	15 s 15 s	MRI	22% 55%
(Huber et al., 2014)	Human	N/A	Visual	30 s	MRI	10%

[a] Relative CBVv change = 100 × (CBVv active – CBVv baseline)/(CBVv baseline) %.

from fast flowing blood water spins (Le Bihan et al., 1988; Silva et al., 1997; Ye et al., 1997). Thus, absolute CBVa can be estimated from the difference signals between images with and without such crusher gradients (Barbier et al., 2001; Duong and Kim, 2000; Kim and Kim, 2006; Neil and Ackerman, 1992; Petersen et al., 2006; van Westen et al., 2011). As flow-sensitized field gradients can only dephase MR signals from moving spins with velocities above a certain threshold, CBVa values measured by this type of method may have substantial contributions from large arteries. One possible solution is to add crusher gradients in the control scan as well. Additionally, as blood flow velocities in larger venules and veins may become close to those in arterioles and small arteries, CBVa values in these methods might also have some contributions from venous vessels.

A second type of approach to isolate the arterial compartment based on blood velocity is to use the multiphase balanced steady state free precession (bSSFP) MRI sequence (Kim et al., 2016; Yan et al., 2012). The bSSFP pulse train has little effect on the longitudinal magnetization of the fast flowing arterial blood water spins as such spins only experience a small number of RF pulses in the bSSFP readout. Meanwhile, the static tissue signal within the imaging volume is saturated by the entire bSSFP pulse train, allowing the quantification of CBVa.

Finally, velocity-selective RF pulse trains (Duhamel et al., 2003; Wong et al., 2006) may be another promising technique that can be exploited to measure CBVa separately based on its faster blood velocity (Liu et al., 2017a).

Approaches based on the impermeability of arterial vessels to exogenous or endogenous contrast agents and arterial spin labeling (ASL)

In healthy brain parenchyma, arterial vessel walls are impermeable to water molecules and many exogenous contrast agents (Lucotte et al., 2017). Water exchange between the intra- and extra-vascular compartments in brain tissue primarily occurs in the capillary bed (Kuschinsky et al., 1996), affecting the signals in the capillaries and downstream venous vessels, and the brain tissue surrounding these vessels. Therefore, volume information in the arterial compartment (CBVa) can be extracted by measuring the signals from intravascular tracers in arterial vessels. For instance, in PET studies, ^{15}O-labeled carbon monoxide (C^{15}O) is a non-diffusible tracer (does not enter extravascular space surrounding all vessels) that can furnish information on CBVtot. On the other hand, ^{15}O-labeled water (H^{15}O) is a tracer that is diffusible in capillaries. Using a two-compartment model, Ito et al. showed that CBVa can be measured with dynamic H^{15}O PET (Ito et al., 2001).

In MRI, magnetically labeled blood water spins can be adopted as endogenous tracers that are impermeable to arterial vessel wall but can diffuse freely across the blood brain barrier in capillaries, such as the arterial spin labeling (ASL) methodology (Detre et al., 1992; Williams et al., 1992). In principle, CBVa can be estimated from the difference signal between the label and control scans in ASL when the post-labeling delay (PLD) is short (Chappell et al., 2010; Warnert et al., 2015; Whittaker et al., 2017), or from the difference ASL signals acquired at multiple PLDs (Chappell et al., 2010; Hales et al., 2013). A series of other ASL based CBVa approaches have been developed.

To separate extravascular tissue and arterial blood signals so that CBVa can be measured, the tissue signal needs to be manipulated. The modulation of tissue and vessel (MOTIVE) method developed by Kim et al. uses magnetization transfer (MT) to saturate the extravascular tissue signal at several different power levels (Kim and Kim, 2005). As the blood signal is minimally affected by MT saturation (Balaban et al., 1991; Hua et al., 2009a), tissue and blood signals can be separated. Meanwhile, the blood signal can be tagged using ASL approaches. The signal contribution from venous blood is minimal here because: 1) the T2 value of venous blood at high field (9.4T) is short (5–7 ms); and 2) the labeled blood water magnetization is close to fully recovered in the venous compartment due to the long transit time for the labeled blood water spins to reach the venous vessels. Therefore, CBVa can be quantified by the MOTIVE approach. Exogenous contrast agents such as MION can also be used to label the blood signal in the MOTIVE method (Kim and Kim, 2005). A second approach is based on the fact that the tissue perfusion signal in ASL (the difference signal between the label and control scans in ASL in the tissue compartment) can be suppressed using the Look-Locker echo-planar imaging (LL-EPI) readout when high flip angle and short spacing are used (Brookes et al., 2007; Francis et al., 2008). Such progressive saturation of the tissue perfusion signal ensures that the measured ASL difference signal originates predominantly from the arterial compartment, thus allowing absolute CBVa to be fitted from the time course sampled with LL-EPI. Vazquez et al. demonstrated another method in which the extravascular tissue signal is nulled using a spin preparation scheme consisting of spatially selective saturation on the imaging slice followed by a series of non-selective inversions (Vazquez et al., 2006). The timing of the non-selective inversion pulses are carefully designed so that the MR signals from gray matter (GM), white matter (WM) and cerebrospinal fluid (CSF) are nulled when images are acquired, leaving the signal from the inflowing arterial blood outside of the slice-selective saturation the predominant detectable component.

Instead of modulating the extravascular tissue signal, one can also

manipulate the blood signal in arterial vessels. In the inflow-based vascular-space-occupancy (iVASO) approach (Hua et al., 2009b, 2011a), arterial blood signal is nulled by spatially selective inversion of the blood water spins flowing into the imaging slice (similar to ASL and slab-selective VASO (Jin and Kim, 2008)) and acquisition of MR images when the inverted inflowing blood water magnetization crosses zero (nulled) during T1 recovery. Thus, by measuring the residual tissue and post-arterial blood signals, relative changes in CBVa during functional stimulation can be inferred. Furthermore, when subtracting with a subsequent scan without arterial blood nulling, absolute CBVa can be quantified on a voxel-by-voxel basis (Donahue et al., 2009a, 2010; Hua et al., 2009c; Hua et al., 2011b; Rane et al., 2016). To account for the heterogeneity of arterial transit times in different brain regions, the iVASO difference signals can be measured at a series of post-labeling delays (PLD) or inversion times (TI), from which absolute CBVa and arterial transit times can be fitted based on a biophysical model developed for the iVASO signal (Hua et al., 2011b). Alternatively, the arterial blood signal can also be tagged using the pseudocontinuous ASL (pCASL) technique (Dai et al., 2008), as demonstrated in the arterial volume using arterial spin tagging (AVAST) approach (Jahanian et al., 2015), to measure relative changes in CBVa during functional stimulation. In AVAST, the images are acquired immediately after the pCASL labeling module (i.e. at a PLD of zero). When the repetition time (TR) and labeling duration in the pCASL labeling module are carefully adjusted according to the vascular transit times in different subjects and brain regions, the tissue signal can be identical in the tag and control scans, while the arterial blood signal is at steady state maximum in the tag scan and zero in the control scan. CBVa can then be determined by subtracting out the tissue signal.

In this type of CBVa method, flow-sensitive crusher gradients can be incorporated to remove fast flowing blood signals in large arteries (Hua et al., 2011b). Thus, CBVa measured in these methods can be sensitized predominantly to small pial arteries and arterioles. Nevertheless, the permeability of the arterial vessel walls may be altered in diseases, which should be taken into consideration when interpreting the measured CBVa values in such conditions. To mitigate this problem, the water permeability effects can be incorporated into existing theories for CBVa quantification. For instance, a water extraction fraction parameter is included in the iVASO model to account for such effects (Hua et al., 2011b). Another disadvantage of all ASL based methods is that it is difficult to measure CBVa when the arterial transit time becomes longer than the typical range of 1–2 s, such as in normal WM or diseased tissue. By the time when the labeled arterial water spins perfuse the entire arterial compartment, the difference in the inflowing blood water magnetization between the label and control scans will be too small for detection due to T1 recovery.

Approaches based on the blood oxygenation level

The oxygenation level of arterial blood in healthy brain parenchyma is usually above 95%, while the venous blood oxygenation level is much lower (Vazquez et al., 2010). In MRI, the transverse relaxation times (T2*/T2) of blood are highly sensitive to such oxygenation level difference (Lu et al., 2012; Zhao et al., 2007). Based on this property, Huber et al. used simultaneous multi-echo BOLD and VASO MRI to measure dynamic changes in CBVa and CBVv during a visual stimulation in humans (Huber et al., 2014). An increase of approximately 55% in CBVa during stimulation compared to baseline CBVa values was observed, in good agreement with results from similar studies using other CBVa methods (Table 3).

None of the MRI approaches discussed in this section require the injection of exogenous contrast agents. Some of the approaches were only demonstrated for the measurement of relative CBVa changes (Huber et al., 2014), while the others can measure absolute CBVa in the brain.

Venous cerebral blood volume (CBVv)

The anatomy and physiology of venous blood vessels are quite different from those of arterial vessels (Schaller, 2004). Arterial vessels are the major active regulator of CBF, while venous vessels mostly dilate passively to accommodate changes in CBF. In addition to being an important indicator for the homeostasis of the venous compartment in the microvasculature, CBVv is known as a strong modulator of the BOLD signal (Buxton and Frank, 1997; Ogawa et al., 1993; van Zijl et al., 1998), which is primarily induced by the susceptibility effects from deoxyhemoglobin in venous blood. Therefore, the measurement of CBVv is critical for the interpretation of microvascular and metabolic origins of the overall BOLD signal differences observed across subjects and in different physiological and pathological states.

In healthy brains, the blood in venous vessels is partially deoxygenated (typically around 60% oxygen saturation), while the blood in arterial vessels is usually close to fully oxygenated (typically >95% oxygen saturation) (Vazquez et al., 2010). Most CBVv MRI methods developed to date rely on such oxygenation level difference to separate venous blood vessels from the rest of microvasculature. Therefore, CBVv measured by these methods reflects the signals from vessels with partially deoxygenated blood, sometimes referred to as the deoxygenated blood volume (DBV) (He and Yablonskiy, 2007). This may include contributions from capillaries, venules and veins. At basal state, CBVv is approximately 70–80% (Table 2) of CBVtot (Piechnik et al., 2008; Sharan et al., 1989; van Zijl et al., 1998). During functional stimulation, the relative change in CBVv is usually smaller than that in CBVa, especially when the duration of the functional stimulation is short (Table 4). CBVv change may increase during longer functional stimuli (Akgoren and Lauritzen, 1999; Chen and Pike, 2009a; Kim and Kim, 2011; Stefanovic and Pike, 2005), or during physiological stimulation such as breathhold (Hua et al., 2010) or hypercapnia (Chen and Pike, 2010; Lee et al., 2001).

Since all CBVv MRI approaches that will be discussed in Section 3 use blood oxygenation level to separate venous blood vessels from arterial vessels, these methods are organized based on the type of technology utilized.

Venous refocusing for volume estimation (VERVE)

Stefanovic et al. developed the VERVE fMRI method for the measurement of relative CBVv change during functional stimulation in the brain (Stefanovic and Pike, 2005). It is based on the fact that the refocusing interval of a Carr-Purcell Meiboom-Gill (CPMG) pulse sequence (τ_{CPMG}) only affects the T2 value of deoxygenated blood, but not T2 of oxygenated blood and extravascular tissue. That is, even as the effective echo time (TE) remains the same, the apparent T2 value of deoxygenated blood increases when τ_{CPMG} decreases. Thus, the deoxygenated blood signal can be isolated by comparing signals from two consecutive scans following CPMG preparations with the same TE but different τ_{CPMG} (3.7 and 30 ms). The difference signal can then be converted to relative CBVv change using a calibration curve of blood T2 and oxygenation level if the venous blood oxygenation levels are known at baseline and during activation. During a flashing checker-board visual stimulation with a long stimulus duration (240 s), VERVE fMRI measured an approximately 16% CBVv increase from baseline in the visual cortex of healthy human brains (Stefanovic and Pike, 2005).

Approaches based on the sampling of the spin echo signal

These approaches exploit the mesoscopic magnetic field inhomogeneities induced by deoxyhemoglobin in blood vessels (Yablonskiy and Haacke, 1994) to measure absolute CBVv. This can be achieved by sampling the exponential signal decay around the spin echo signal using the gradient echo sampling of spin echo (GESSE) sequence (Yablonskiy, 1998; Yablonskiy and Haacke, 1997) or the multi-echo gradient and spin echo sequence (MEGESE) (An and Lin, 2000, 2002a,

b), or the asymmetric spin echo sequence (An and Lin, 2003). Because such methods are sensitive to background macroscopic field inhomogeneity which can be much larger than the oxygenation-induced susceptibility shifts, an extra field map (B0) scan is usually needed to correct for this macroscopic inhomogeneity (An and Lin, 2002a). Compared to earlier studies, the quantitative BOLD (qBOLD) theory (He and Yablonskiy, 2007; He et al., 2008) is a more realistic model that was expanded to include contributions from multiple tissue compartments. One advantage of this type of method is that additional physiological parameters such as the oxygen extraction fraction (OEF) can also be quantified with the same data and equations (Lin and Powers, 2017). It should be noted that most BOLD models used in these approaches assume static dephasing regime without accounting for the molecular diffusion effects around capillaries (Fujita, 2001; Kiselev and Posse, 1999), which may lead to an underestimate of CBVv (Dickson et al., 2011; He and Yablonskiy, 2007). Besides, it has been shown that interdependence exists between CBVv and OEF in the models, which makes it difficult to fit these two parameters separately from the spin echo signal alone (Sedlacik and Reichenbach, 2010). Moreover, in patients with abnormal hemo-metabolic coupling, assumptions of relationships between these parameters are often altered compared to healthy subjects. Some of these issues (diffusion around capillaries, interdependence of parameters) are being addressed in more recent on-going developments (Christen et al., 2012, 2011, 2014; Dickson et al., 2011).

T2-based multi-echo approaches*

Multi-echo MRI sequences can be used to measure T2* values which are highly sensitive to blood oxygenation level difference (Lu et al., 2012; Zhao et al., 2007). Using simultaneous multi-echo BOLD and VASO MRI, Huber et al. reported a 10% increase in CBVv (relative to baseline CBVv) during a visual stimulation in humans (Huber et al., 2014). Havlicek et al. found that the intercept from a linear fitting of the multi-echo BOLD signals may be a good estimate for dynamic changes in CBVv (Havlicek et al., 2017).

Approaches using gas-inhalation

Hypercapnic and hyperoxic gas mixtures are potent modulators of the blood oxygenation level, and thus can be used as endogenous tracers to measure perfusion. By modulating CO2 (typically 2–7%) and O2 (typically 30–100%) content in inspired gas within the typical physiological range, hypercapnia and hyperoxia can be induced safely in human subjects during MRI scans (Brueckl et al., 2006; Donahue et al., 2014; Spano et al., 2013). Inhalation of a hyperoxic gas mixture reduces the concentration of deoxyhemoglobin in blood vessels without significant vasodilation or vasoconstriction effects (thus no substantial CBV and CBF changes) and without significant changes in oxygen consumption (Diringer et al., 2007; Mark and Pike, 2012; Xu et al., 2012). Thus, the MR signal change associated with the change in the concentration of deoxyhemoglobin can be utilized to measure blood volume information. As the arterial blood is usually close to fully oxygenated during normoxia in healthy brain, such manipulation of deoxyhemoglobin (ratio between deoxyhemoglobin and oxyhemoglobin) predominately affects blood in capillaries, venules and veins, and thus allows the estimation of CBVv.

Bulte et al. demonstrated the feasibility of this type of method by acquiring gradient echo (GRE) EPI BOLD images during interleaved normoxia and hyperoxia blocks (Bulte et al., 2007a, 2007b). Absolute CBVv can be calculated from the ratio of steady-state tissue signals during the hyperoxia and normoxia periods, normalized by the same ratio from a pure blood voxel (sagittal sinus). Blockley et al. later showed that the normalization step may introduce additional error due to variations of baseline physiological parameters such as hematocrit and OEF (Blockley et al., 2013a). Instead, a quantitative model based on an empirical relationship between CBVv, and the BOLD signal change, PaO2 change and echo time (TE) was proposed, which does not require a normalization step with signals from a pure blood voxel. More recently, Liu et al. proposed a concomitant O2 and CO2 gas inhalation paradigm which can measure CBVv along with several other hemodynamic parameters from the BOLD images (Liu et al., 2017b). Blockley et al. also showed that relative changes in CBVv during functional stimulation can be measured using gas-inhalation based methods with typical temporal resolution for fMRI studies (Blockley et al., 2012). In addition, average venous vessel size can be quantified using a simultaneous gradient echo and spin echo sequence during hypercapnia and hyperoxia (Germuska and Bulte, 2014; Jochimsen et al., 2010; Shen et al., 2013).

The advantages of the gas-inhalation based approaches include complete noninvasiveness, and wide availability of the MRI pulse sequences for whole brain acquisition (basically BOLD fMRI sequences) on most modern clinical MRI systems. Moreover, with proper design of pulse sequence and/or gas-inhalation paradigm, additional physiological parameters such as CBF and cerebrovascular reactivity (CVR) can be extracted from one single scanning session (Bulte et al., 2007a; Liu et al., 2017b), which substantially improves its relevance as a multi-parametric clinical protocol capable of sampling multiple hemodynamic compensation mechanisms.

Several confounding effects may need to be considered when designing the protocol for gas-inhalation based CBVv methods and when interpreting the results. It should be noted that hyperoxia can induce a number of physiological and biochemical changes in the blood, such as the partial pressures of O2 and CO2, the acidity of the blood, and the binding of O2 and CO2 with hemoglobin (Becker et al., 1996; Bulte et al., 2007a; Christiansen et al., 1914; Jensen, 2004; Johnston et al., 2003a, 2003b; Poulin et al., 1998; Watson et al., 2000). Here, when using hyperoxia as a contrast agent for the measurement of CBVv, its effects on CBF and CMRO2 are the most relevant. First, CBF is assumed to remain constant during hyperoxia in current models. However, the increase in blood O2 levels (Bulte et al., 2007b) and the accompanying decrease in blood CO2 levels (Iscoe and Fisher, 2005) during hyperoxia may cause CBF reduction, which will generally lead to an overestimate of CBVv from the BOLD signal (Blockley et al., 2013a). This confound can be minimized by keeping the duration of gas inhalation relatively short, or by accounting for blood O2 and CO2 changes in the analysis (Liu et al., 2017b; Mark and Pike, 2012; Xu et al., 2012). Second, hyperoxia is usually considered a global vascular challenge which is not expected to elicit neuronal activity. Therefore, CMRO2 is also assumed to remain constant during hyperoxia in current models. However, there are still debates on this question with studies from the literature showing increase (Rockswold et al., 2010), decrease (Richards et al., 2007; Xu et al., 2012), or same (Diringer et al., 2007) CMRO2 during hyperoxia compared to normoxia. An increase in CMRO2 during hyperoxia will result in an overestimate of CBVv with current theories, and vice versa (Blockley et al., 2013a). This issue warrants further investigation, and the CMRO2 response during hyperoxia may alter under different physiological and pathological conditions. Finally, extreme hyperoxia may reduce blood water T1 values (Siero et al., 2015), which may confound T1-weighted effects in the MR signals.

None of the MRI approaches discussed in this section requires the injection of exogenous contrast agents. Some of the approaches were only demonstrated for the measurement of relative CBVv changes (Blockley et al., 2012; Havlicek et al., 2017; Huber et al., 2014; Stefanovic and Pike, 2005), while the others can measure absolute CBVv in the brain.

Efforts in the investigation of flow-volume coupling in arterial and venous blood vessels

The coupling between CBF and CBV has been a fundamental question in physiology, and has been the topic for numerous studies in human and animal brains. To date, the power law relationship $CBV = 0.80 \times CBF^{0.38}$ from the seminal work by Grubb et al. (1974) in anesthetized rhesus monkeys with varying arterial CO2 tension is still widely used in

quantitative theories for understanding the BOLD effect and for modeling the microvasculature. Nevertheless, accumulating evidence shows that this relationship may vary with many factors (Kida et al., 2007; Rostrup et al., 2005; Wu et al., 2002), such as species and brain region; stimulus type, strength and duration; transient or steady state signals, and many others. As we discussed above, arterial and venous blood vessels have intrinsically different physiological and functional roles in the brain. Therefore, the flow-volume coupling may also differ in the arterial and venous compartments. As capillary blood is partially deoxygenated, capillaries are considered part of the venous compartment in this discussion. Here, we define CBVtot = CBVa + CBVv, and thus only two of the three parameters in the equation need to be independently measured. Main results in the literature are summarized in Table 5 (again, we only included studies that measured CBVa and/or CBVv separately, but not CBVtot).

Using the blood velocity based method developed by (Duong and Kim, 2000), Lee et al. measured CBVa and CBVv in rat brains during normoxia and hypercapnia (Lee et al., 2001). The coupling between CBF and CBVtot ($CBVtot \sim CBF^{0.40}$) was found to be similar to (Grubb et al., 1974), which can be linearized ($\Delta rCBVtot/\Delta rCBF = 0.31$) in the typical CBF range in the brain. The flow-volume coupling was significantly different in the arterial ($\Delta rCBVa/\Delta rCBF = 0.79$) and venous ($\Delta rCBVv/\Delta rCBF = 0.15$) compartments.

Kim et al. measured CBVa and CBF using the MOTIVE method (Kim and Kim, 2005) and CBVtot in the somatosensory cortex of rat brains during forepaw stimulation (Kim et al., 2007). The following flow-volume relationships were reported: $\Delta rCBVtot/\Delta rCBF = 0.45$ and $\Delta rCBVa/\Delta rCBF = 1.86$. The flow-volume coupling during a neuronal activation (forepaw stimulation here) seemed to be substantially different from the relationships measured during a vascular challenge (hypercapnia) that is not expected to elicit significant neuronal activation (Lee et al., 2001). In addition, different vascular tone in different anesthesia (α-chloralose vs isoflurane) may contribute to the difference as well. However, in both studies, the relative contributions from the arterial compartment were much greater than the venous compartment.

Chen et al. applied the VERVE method (Stefanovic and Pike, 2005) to measure relative CBVv changes during neuronal activation (simultaneous finger tapping and flashing checkerboard presentation) (Chen and Pike, 2009a) and vascular stimulation (graded hypercapnia and hypocapnia) (Chen and Pike, 2010). They reported the following relationships between CBF and CBVv: $CBVv \sim CBF^{0.23\pm0.05}$ during neuronal activation, and $CBVv \sim CBF^{0.18\pm0.02}$ during vascular stimulation. In addition, they found that the power coefficients were relatively homogeneous across different brain regions.

Hua et al. employed iVASO, VASO and ASL MRI to monitor the responses of CBVa, CBVtot, and CBF, respectively, in human visual cortex during brief breath-hold (vascular challenge) and visual stimulation with identical stimulus duration (15 s) (Hua et al., 2010, 2011c). CBVv was calculated from the difference between CBVtot and CBVa. The results have been reported in abstract form (Hua et al., 2010), and are summarized here in Table 6 and Figs. 1 and 2. First (comparing across task), the relative change in CBVtot ($\Delta CBV/CBV_{baseline}$) during breath-hold was found to be twice as large as that during visual stimulation, whereas relative CBVa change was comparable between the two tasks. This suggests that the larger CBVtot change during breath-hold may originate primarily from CBVv. Previous human (Donahue et al., 2009b) and animal studies (Mandeville et al., 1998) also reported greater CBVtot change during hypercapnia than during neuronal activation. Second (comparing across vascular compartment, i.e. CBVa and CBVv), the relative increases in CBVa, CBVv and CBVtot during breath-hold were comparable, whereas during visual stimulation, CBVa rose twice as much as CBVv, and CBVv change was smaller than CBVtot change. Thus, the dilation in the arterial compartment accounted for approximately 20% and 40% of CBVtot increase during breath-hold and visual stimulation, respectively. This observation is in congruence with prior results from animal studies (Kim et al., 2007; Lee et al., 2001). Finally, the relative CBF changes were comparable between the two tasks. This indicates that the coupling between CBVtot/CBVv and CBF differed markedly between breath-hold and visual stimulation, whereas the power law relationship between CBVa and CBF was largely preserved during both tasks, which can be expected as CBF is primarily controlled by arterial vessels (Table 5, Fig. 2). According to the central volume theorem (flow = volume/transit time), these data also imply that the reduction in arterial transit times (calculated from CBF and CBVa) during both stimuli were small (5–10%), while the changes in mean transit times (calculated from CBF and CBVtot) were larger during visual stimulation (≈25%) than during breath-hold (5–10%). Similar observations were reported in rat brains (Kim et al., 2007). For instance, Meng et al. reported that blood

Table 6
Relative changes in CBF, CBV, CBVa and CBVv in human visual cortex during breathhold and visual stimulation reported in a previous study.

ΔS/S (%)	CBF	CBV	CBVa	CBVv
Breathhold	60.8 ± 7.2	54.9 ± 5.8	53.1 ± 6.2	54.5 ± 4.9
Visual	62.5 ± 7.5	28.2 ± 5.2	53.6 ± 5.5	22.2 ± 3.8

This table summarizes results from a previous study that has been presented in abstract form (Hua et al., 2010). iVASO, VASO and ASL MRI were employed to monitor the responses of CBVa, CBVtot, and CBF, respectively, in human visual cortex during a 15-s breathhold and a 15-s visual stimulation. More experimental details can be found in (Hua et al., 2010, 2011c).
ΔS/S = (S active – S baseline)/(S baseline).
n = 10, mean ± standard deviation. The standard deviations represent inter-subject variations.

Table 5
Relationship between CBF and CBV changes during functional and physiological stimulation in arterial and venous vessels reported in the literature.

Reference	Species	Anesthesia	Stimulation		Technique	Flow-volume coupling
			Type	Duration		
(Lee et al., 2001) **$CBVtot \sim CBF^{0.40}$ or $\Delta rCBVtot/\Delta rCBF = 0.31$, $\Delta rCBVa/\Delta rCBF = 0.79$, $\Delta rCBVv/\Delta rCBF = 0.15$**	Rat	α-chloralose	Hypercapnia	N/A	19F NMR, microscopy	
(Kim et al., 2007) **$\Delta rCBVtot/\Delta rCBF = 0.45$ and $\Delta rCBVa/\Delta rCBF = 1.86$**	Rat	isoflurane	Forepaw stimulation	15 s	MRI	
(Chen and Pike, 2009a) **$CBVv \sim CBF^{0.23\pm0.05}$**	Human	N/A	Visual and sensorimotor	96 s	MRI	
(Chen and Pike, 2010) **$CBVv \sim CBF^{0.18\pm0.02}$**	Human	N/A	Hypercapnia, hypocapnia	180 s	MRI	
(Hua et al., 2010; Hua et al., 2011c) **$CBVtot \sim CBF^{0.52\pm0.04}$, $CBVa \sim CBF^{0.86\pm0.05}$, $CBVv \sim CBF^{0.42\pm0.03}$**	Human	N/A	Visual	15 s	MRI	
(Hua et al., 2010; Hua et al., 2011c) **$CBVtot \sim CBF^{0.90\pm0.05}$, $CBVa \sim CBF^{0.86\pm0.05}$, $CBVv \sim CBF^{0.90\pm0.05}$**	Human	N/A	Breathhold	15 s	MRI	

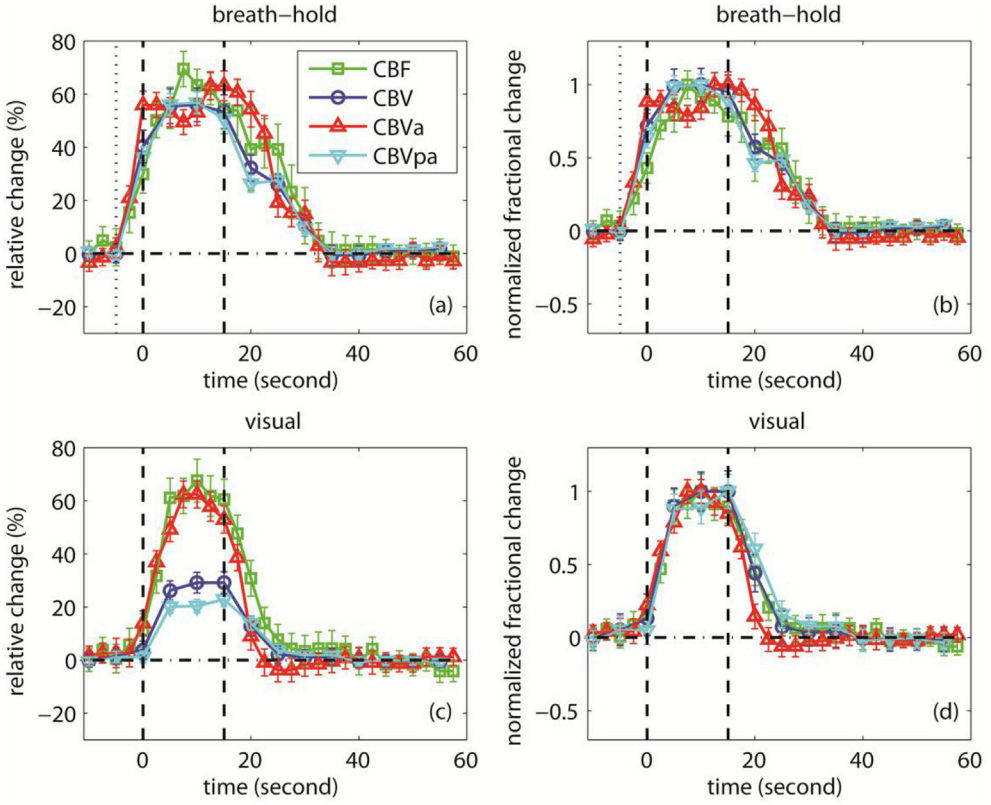

Fig. 1. Results from a previous study that has been reported in abstract form (Hua et al., 2010). The average time courses of CBF, CBV, CBVa and CBVv evolution during breathhold (a, b) and visual (c, d) experiments are shown. The error bars represent inter-subject standard deviation (n = 10). The relative signal changes (ΔS/S) were displayed in (a, c). For better visualization and easier comparison, each time course in (a, c) was normalized by their individual maximum change (scale 0–1) and displayed in (b, d), respectively. The standard deviations were scaled accordingly. The vertical dotted lines in (a, b) represent the beginning of exhaling before breathhold. The vertical dash lines in (a–d) describe the start and end of the stimulation period. More experimental details can be found in (Hua et al., 2010, 2011c).

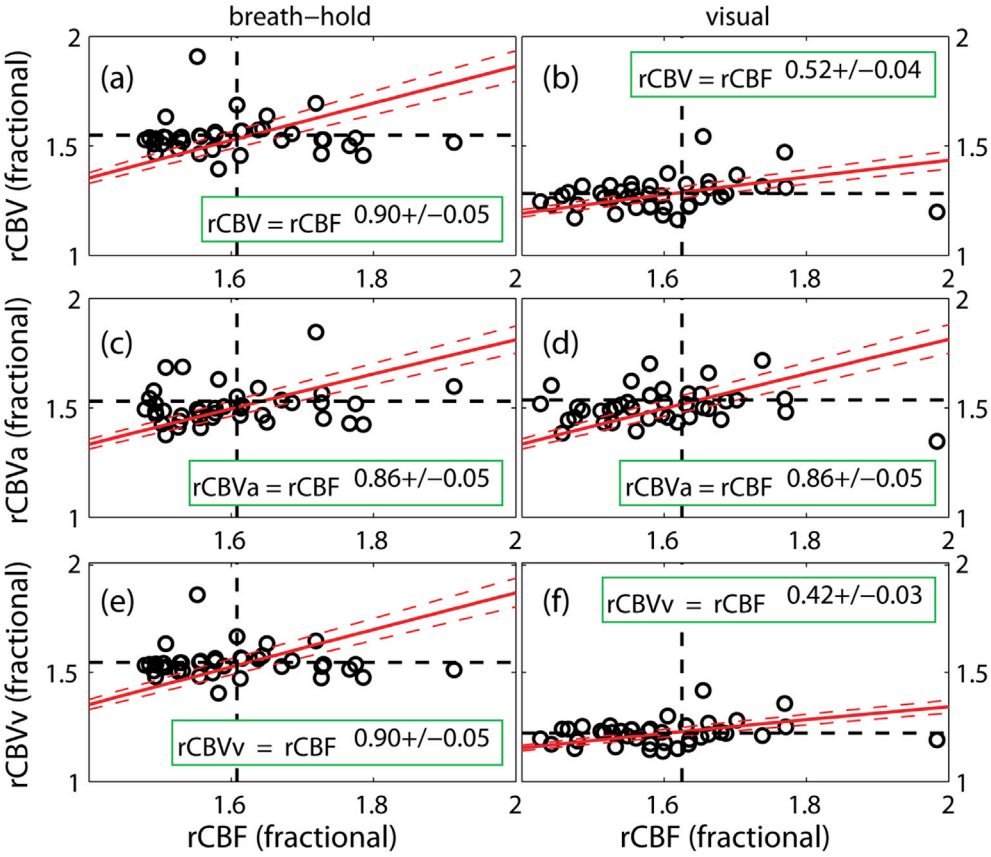

Fig. 2. Results from a previous study that has been reported in abstract form (Hua et al., 2010). The power law relationships between relative CBV/CBVa/CBVv and CBF during breathhold (a, c, e) and visual stimulation (b, d, f) are shown. Relative CBV (rCBV) and CBF (rCBF) are defined as the parameters normalized by their respective baseline values. Linear regression was performed to fit for each α (n = 40). The standard deviations represent the 95% confidence intervals. More experimental details can be found in (Hua et al., 2010, 2011c).

transit times from carotid arteries to cortical arterial vessels and to capillaries (similar to arterial transit time) were not significantly changed during forepaw stimulation in rat brains (Meng et al., 2012).

The results summarized above showed considerable variations, which warrants further investigation. This may be due to various confounding factors such as species, use of anesthesia in animal studies (Meng et al., 2012), brain region, spatial resolution, stimulus type, strength and duration, CO2 inhalation and breath-hold which may induce different hypercapnic conditions (Bulte et al., 2009), and the technologies used to measure the parameters. Kida et al. also reported that such relationship may vary substantially during the transient period after stimulation onset (Kida et al., 2007). Nevertheless, it seems to be clear that the flow-volume coupling may differ substantially in the arterial and venous compartments. Therefore, independent measurements of CBVa and CBVv should furnish more accurate and robust results, as compared to the commonly adopted procedure that estimates CBV change from CBF measure using a power law relationship.

These results also reiterate the importance of CBVv change in the calibrated fMRI method that uses hypercapnia as a calibration state to quantify CMRO2 change during neural activation (Blockley et al., 2013b; Davis et al., 1998; Hoge et al., 1999), which has been pointed out in previous studies (Kim et al., 1999). First, the calibrated fMRI method usually assumes that the flow-volume coupling is identical during focal neuronal activation and global vascular stimulation. Second, it also assumes that CBVv change, which has dominant effects on the overall BOLD signal, may be approximated with CBVtot change, which may be easier to measure by many existing techniques. This historical assumption is based on the general belief that CBVa change is negligible during functional stimulation (Buxton et al., 1998; Mandeville et al., 1998, 1999), mainly because CBVa occupies only around 20–30% of CBVtot at baseline (Table 1). However, as we discussed in section 2, accumulating evidence showed that the largest relative vasodilation during neuronal activation occurs in arterioles, which may account for 30–60% of the CBVtot increase. Furthermore, at higher fields, CBVa changes are also likely to modulate the BOLD signal in significant ways (Tong et al., 2018; Uludag et al., 2009). Therefore, for accurate CMRO2 quantification using calibrated fMRI, individual CBVa and CBVv measurements during both stimuli may be necessary, and the signal contribution from the arterial compartment may need to be incorporated into the theory (Griffeth and Buxton, 2011).

Clinical applications

As many of the CBVa and CBVv MRI approaches described above have only been developed recently, reports for their applications in clinical and basic science studies are currently limited in the literature. Nevertheless, pilot results from several studies have demonstrated potential value to measure microvascular changes in specific segments of the vascular tree.

Arterial steno-occlusive disease

CBVa may be an important microvascular parameter to monitor in arterial steno-occlusive disease in the brain, and can be affected both in patients with cervical and intracranial arterial stenosis (the major risk factors for new or recurrent stroke) (Donahue et al., 2017). Autoregulatory response to decreased cerebral perfusion pressure in the early stage of the disease may result in arterial dilation (thus CBVa increase) to maintain adequate CBF (Derdeyn et al., 2002). Using iVASO MRI, Donahue et al. measured middle cerebral artery territory CBVa in patients with mild ($n = 7$) and severe ($n = 10$) extracranial internal carotid artery (ICA) stenosis (Donahue et al., 2010). Slightly increased GM CBVa was observed in these patients compared to healthy controls. In addition, significant difference in CBVa between the left and right hemispheres was observed in the patients but not in the controls.

Brain tumor

Angiogenesis is a critical step of tumor growth (Folkman, 1995), which results in altered number of blood vessels, and thus abnormal CBVtot in tumoral regions. Therefore, tumor CBVtot is a perfusion measure that has demonstrated essential diagnostic value for predicting tumor grade and response to therapeutics (Law et al., 2004). Dynamic susceptibility contrast (DSC) MRI is currently the standard clinical MRI scan for measuring brain tumor perfusion parameters such as CBVtot and CBF (Cha et al., 2002). It was shown that arterioles may generate before capillaries and venous vessels in angiogenesis (Hansen-Smith et al., 2001). Therefore, tumor CBVa may be a more specific measure for tumor perfusion. Several studies have measured CBVa with different MRI methods in brain tumor patients. All studies so far showed increased CBVa with tumor grade, and correlation between CBVa and CBVtot measured with DSC MRI (Hales et al., 2013; van Westen et al., 2011; Wu et al., 2016). In one pilot study with a small cohort of patients (12 brain tumor patients with the World Health Organization (WHO) glioma grades of IV ($n = 3$), III ($n = 3$), and II ($n = 6$)) (Wu et al., 2016), CBVa measured by iVASO MRI showed significant correlation with tumor grade ($\rho = 0.37$, $P = 0.04$), whereas CBVtot measured by DSC MRI in the same patients only showed a trend of correlation with tumor grade ($\rho = 0.28$, $P = 0.5$).

Schizophrenia

Schizophrenia is a devastating psychiatric disorder that affects 0.5–1% of the American population with disabling psychosis, negative symptoms, and cognitive impairment (Mueser and McGurk, 2004). Abnormal CBVtot has been reported in schizophrenia in many brain regions, such as the frontal cortex (Bellani et al., 2011; Peruzzo et al., 2011; Schobel et al., 2009) and the hippocampus (Schobel et al., 2009, 2013; Talati et al., 2016; Talati et al., 2014; Tamminga et al., 2012). However, histological studies of capillary morphology did not find significant changes in postmortem brain tissue from schizophrenia patients (Kreczmanski et al., 2005, 2009; Uranova et al., 2010). Therefore, the CBVtot changes may originate in the other compartments of the microvasculature. Hua et al. adopted the iVASO MRI approach with large-vessel signal crushing and 3D whole brain coverage at 7T to investigate CBVa abnormalities (predominantly small pail arteries and arterioles) in schizophrenia (Hua et al., 2016a). Bilateral GM CBVa changes were detected in patients compared to healthy controls in multiple brain areas, such as multiple frontal and temporal regions (decrease), the cingulate cortex (decrease), and the hippocampus (increase). Significant negative correlations were found between disease duration and GM CBVa in superior temporal gyrus, middle temporal gyrus, and Heschl's (transverse temporal) gyrus. These results were obtained after controlling for age, smoking status, and antipsychotic medication dosage.

Huntington's disease (HD)

Huntington's disease (HD) is a neurodegenerative disease caused by an expanding CAG repeat in the *Huntingtin* gene (Group, 1993; Ross and Tabrizi, 2011). The natural history of HD can be divided into manifest and premanifest periods (of motor symptoms). Mutation positive individuals can be identified by genetic testing many years before manifest HD, which provides the opportunity for therapeutic intervention to prevent or delay irreversible brain damage. Striatal atrophy is currently the most commonly used biomarker for HD (Aylward et al., 2012; Paulsen et al., 2010; Tabrizi et al., 2009). Microvascular and metabolic changes in the brain may occur earlier and may progress more rapidly than structural brain changes (atrophy) in HD (Tang et al., 2013). Indeed, abnormalities in the microvasculature (Drouin-Ouellet et al., 2015; Franciosi et al., 2012; Vis et al., 1998) and CBVtot (Cepeda-Prado et al., 2012; Lin et al., 2010) have been reported in the premanifest stage of HD. Increased release of vascular endothelial growth factor (VEGF), which

regulates vessel growth, has also been observed from mutant *Huntingtin* striatal cells (Niatsetskaya et al., 2010). More recently, Drouin et al. (Drouin-Ouellet et al., 2015) and Hua et al. (2014) both reported significant increase in CBVa in premanifest HD patients compared to healthy controls using two different CBVa MRI approaches (Brookes et al., 2007; Hua et al., 2011b). Significantly elevated CBVa values in the frontal cortex strongly correlated with the projected year-to-onset of motor symptoms estimated from the length of the CAG repeat mutation in patients (Hua et al., 2014). The relative magnitude (% of average control values) of CBVa changes was greater than that of total CBF and brain volumetric measures in premanifest HD patients (Hua et al., 2014). Such alterations in arterial vessels have been linked with the intercellular transportation of mutant *Huntingtin* protein in HD (Drouin-Ouellet et al., 2015).

Alzheimer's disease (AD)

Microvascular dysfunctions have been implicated in the pathophysiology of AD (Iadecola, 2004) at the early stages of the disease (Iturria--Medina et al., 2016). Abnormal CBF (Kisler et al., 2017; Leeuwis et al., 2017; Ostergaard et al., 2013) and CBVtot (Harris et al., 1996; Lacalle-Aurioles et al., 2014; Nielsen et al., 2017; Uh et al., 2010) have been demonstrated by a number of studies in AD. In a mouse model of aging, Balbi et al. showed that pial arteries and arterioles can be affected months before dysfunctions in capillaries and venous vessels were observed (Balbi et al., 2015). Hua et al. applied the iVASO MRI approach at 7T to investigate the volume of small pial arteries and arterioles (CBVa) in the brain at the pre-dementia stage of AD (Hua et al., 2016b, 2017). In the study, 18 subjects with mild-cognitive-impairment (MCI) and 22 cognitively normal controls underwent MRI scans, as well as 11C-Pittsburgh-Compound-B (PiB) PET scans to evaluate Amyloid-beta (Aβ) burden, and a battery of neuropsychological tests for cognitive assessment. The cognitive battery was repeated for each participant two years after the initial visit to assess cognitive decline over the period (2.00 ± 0.76 years). Genotyping of Apolipoprotein E e4 (APOE4), the major genetic risk factor for AD (Corder et al., 1993), was also performed in all participants. Compared to individuals not carrying any e4-allele, the risk for developing AD is increased by a factor of ca. 3 in subjects carrying one e4-allele, and by a factor of ca. 10–30 for homozygote carriers (two e4-alleles). In MCI subjects, CBVa was significantly elevated compared to cognitively normal controls in many brain regions, such as frontal, temporal, motor, insular and olfactory cortex, and the hippocampus, many of which are known as signature regions for neurodegenerative brain changes in AD. Interestingly, many regions with elevated CBVa in MCI overlapped with regions showing increased Aβ-deposition in PiB PET scans in the same subjects. Indeed, recent studies revealed that pial arteries act as the main entry point for the transportation of protein aggregates from brain tissue to the circulatory system (Iliff et al., 2012). Further statistical analysis in this study showed that CBVa and Aβ-burden measured at baseline (the initial visit) synergistically predicted cognitive decline in these subjects over two years. Moreover, CBVa values in the orbitofrontal cortex showed a significant correlation with APOE4 carrier status in both MCI subjects and controls. Collectively, these results suggested the potential value of measuring CBVa in AD, which may be a potential biomarker in its early stage, and more importantly, may shed light on the pathophysiology of the disease, linking abnormalities in arterial blood vessels and Aβ clearance, and their synergetic effects on cognitive impairment.

Hypertension

Hypertension affects the lumen of arterial vessels (Baumbach and Heistad, 1988; Laurent et al., 2005), and thus may change CBVa. It has been reported that the structure of arteriolar vessels is altered by hypertension, whereas venules are unchanged (Harper and Bohlen, 1984). Recent studies showed that the arterial transit time was prolonged in untreated hypertensive subject compared with normotensive subjects, while similar CBF was observed between the two groups (Lee and Kim, 2017), suggesting increased CBVa due to auto-regulatory process to maintain sufficient perfusion. This implies that CBVa may be a sensitive indicator for early hypertension-induced cerebrovascular impairments. As the disease progresses, the damage in the cerebrovasculature worsens over time. In severely hypertensive rats (over 200 mmHg), CBF was significantly reduced in comparison with moderately hypertensive animals which had similar CBF values as control animals (Yamori and Horie, 1977). Another study showed that vascular resistance in small arteries and arterioles was higher in the established phase of hypertension than those in newly developed hypertension (Pires et al., 2013). These findings suggest that contributions from different segments of the microvasculature to the cerebral abnormalities in hypertension may vary in different stages of the disease.

Epilog and perspective

Since its invention, MRI has evolved from a structural imaging technique to a versatile and powerful tool that can probe various key biophysical and physiological parameters in the human body. One of the main themes in the development of modern MRI technologies has been the continual improvement of the biological and physiological specificity of MRI measures. The MRI techniques discussed in this review that can quantify arterial and venous CBV separately represent the efforts to measure further details of the elaborate microvasculature, one step forward from the relatively established total CBV and CBF MRI approaches.

A critical next step is to validate the arterial and venous specificity of these methods with gold standard technologies. Most studies to date compared their measured CBVa and CBVv values with corresponding values estimated using other imaging modalities. Some studies examined the correlation between CBVa measured using their methods and CBVtot measured with DSC MRI (Donahue et al., 2010; Hales et al., 2013; Kim and Kim, 2005; van Westen et al., 2011; Wu et al., 2016). The transverse relaxation times (T2*/T2) of blood are highly oxygenation level dependent (Lu et al., 2012; Zhao et al., 2007). In iVASO MRI, the predominant arterial origin was validated by measuring the T2*/T2 values of the iVASO difference signal (Hua et al., 2011b), as arterial blood T2*/T2 is distinct from that of capillary and venous blood, as well as the extravascular tissue and CSF. As imaging methods that can separate arterial and venous blood vessels are relatively underdeveloped, it is not trivial to define a gold standard for validation. We think that invasive optical imaging approaches that can selectively label arterial vessels in animal brains (Shen et al., 2012) may serve as an ultimate validation for the MRI methods.

Many of the CBVa and CBVv MRI approaches to date can only acquire one to a few slices within each volume repetition time (TR). To make the techniques useful for applications in clinical studies and neuroscience research, whole brain coverage is essential. With advanced MRI pulse sequences, especially parallel imaging techniques, many of these methods can be expanded to cover larger imaging volumes within one TR. For instance, the iVASO approach was originally developed as a single slice sequence. Recently, it was extended to a 3D whole brain scan using a turbo field echo (TFE, also known as fast GRE) (Hua et al., 2016a) or a gradient spin echo (GRASE) (Rane et al., 2017) readout with typical spatial resolution for perfusion measures and reasonable total scan duration (5–10 min). In addition, the multiband techniques (Setsompop et al., 2012) can be incorporated in many existing sequences to improve spatial coverage and/or acquisition efficiency (Kim et al., 2013; Lee and Kim, 2017).

Blood vessels on the cortical surface and in deep layers as well as the penetrating arterioles and venules between layers may each have intrinsically different roles in the regulation of cerebral perfusion (Blinder et al., 2013; Huber et al., 2014; Tian et al., 2010). To investigate cortical depth-specific microvascular properties, the spatial resolution of the existing CBVa and CBVv imaging techniques needs to be improved

substantially, and new approaches may need to be developed to achieve sub-millimeter resolution. Promising results have been demonstrated to use sub-millimeter CBV-weighted fMRI at ultra-high field (7T) to parse layer-dependent functional signals in human brains (Huber et al., 2017a). We believe that more efforts should be devoted in this regard to push the limits of current CBVa and CBVv MRI approaches.

Most current CBVv MRI approaches cannot separate signals from the capillaries and venules and veins. Although arterioles are believed to be the major regulator of tissue perfusion, several animal studies using optical imaging methods also showed that perivascular control at the capillaries can be faster than arterioles, and that the fractional volume change of the capillaries can outweigh that of the arterioles (Hillman et al., 2007; Tian et al., 2010). Therefore, MRI approaches that can quantify capillary blood volume exclusively may be useful tools for the investigation of capillary specific changes in the microvasculature.

The clinical results reviewed here are limited yet encouraging. The fact that opposite changes in CBVa were measured with the same approach in different diseases (increase in HD (Hua et al., 2014), but decrease in schizophrenia (Hua et al., 2016a)) suggests that the abnormalities observed are not likely due to some undetected systemic bias or artifact. We believe that the continual development of MRI approaches to image different segments of the microvascular tree *in vivo* will allow us to reveal the exquisite details about different types of blood vessels, and their respective effects on the susceptibility to various brain diseases.

Funding

Grant support from NIH R21 EB023538, R21 MH107016, P41 EB015909, K25 HL121192; and the Dana Foundation.

Acknowledgments

We thank Laurentius Huber for his insightful comments on the manuscript. Grant support was provided by the National Institutes of Health (NIH): R21 EB023538, R21 MH107016, P41 EB015909, K25 HL121192; and the Dana Foundation.

References

Akgoren, N., Lauritzen, M., 1999. Functional recruitment of red blood cells to rat brain microcirculation accompanying increased neuronal activity in cerebellar cortex. Neuroreport 10, 3257–3263.
An, H., Lin, W., 2000. Quantitative measurements of cerebral blood oxygen saturation using magnetic resonance imaging. J. Cerebr. Blood Flow Metabol. 20, 1225–1236.
An, H., Lin, W., 2002a. Cerebral oxygen extraction fraction and cerebral venous blood volume measurements using MRI: effects of magnetic field variation. Magn. Reson. Med. 47, 958–966.
An, H., Lin, W., 2002b. Cerebral venous and arterial blood volumes can be estimated separately in humans using magnetic resonance imaging. Magn. Reson. Med. 48, 583–588.
An, H., Lin, W., 2003. Impact of intravascular signal on quantitative measures of cerebral oxygen extraction and blood volume under normo- and hypercapnic conditions using an asymmetric spin echo approach. Magn. Reson. Med. 50, 708–716.
Auer, L.M., Johansson, B.B., 1980. Dilatation of pial arterial vessels in hypercapnia and in acute hypertension. Acta Physiol. Scand. 109, 249–251.
Aylward, E.H., Liu, D., Nopoulos, P.C., Ross, C.A., Pierson, R.K., Mills, J.A., Long, J.D., Paulsen, J.S., Investigators, P.-H., Coordinators of the Huntington Study G, 2012. Striatal volume contributes to the prediction of onset of Huntington disease in incident cases. Biol. Psychiatr. 71, 822–828.
Balaban, R.S., Chesnick, S., Hedges, K., Samaha, F., Heineman, F.W., 1991. Magnetization transfer contrast in MR imaging of the heart. Radiology 180, 671–675.
Balbi, M., Ghosh, M., Longden, T.A., Jativa Vega, M., Gesierich, B., Hellal, F., Lourbopoulos, A., Nelson, M.T., Plesnila, N., 2015. Dysfunction of mouse cerebral arteries during early aging. J. Cerebr. Blood Flow Metabol. 35, 1445–1453.
Barbier, E.L., Silva, A.C., Kim, S.G., Koretsky, A.P., 2001. Perfusion imaging using dynamic arterial spin labeling (DASL). Magn. Reson. Med. 45, 1021–1029.
Barrett, M.J., Tawhai, M.H., Suresh, V., 2012. Arteries dominate volume changes during brief functional hyperemia: evidence from mathematical modelling. Neuroimage 62, 482–492.
Baumbach, G.L., Heistad, D.D., 1988. Cerebral circulation in chronic arterial hypertension. Hypertension 12, 89–95.
Becker, H.F., Polo, O., McNamara, S.G., Berthon-Jones, M., Sullivan, C.E., 1996. Effect of different levels of hyperoxia on breathing in healthy subjects. J. Appl. Physiol. 81 (1985), 1683–1690.
Bellani, M., Peruzzo, D., Isola, M., Rambaldelli, G., Perlini, C., Baiano, M., Cerini, R., Andreone, N., Barillari, M., Mucelli, R.P., Balestrieri, M., Tansella, M., Bertoldo, A., Brambilla, P., 2011. Cerebellar and lobar blood flow in schizophrenia: a perfusion weighted imaging study. Psychiatr. Res. 193, 46–52.
Belliveau Jr., J.W.N.K.D., McKinstry, R.C., Buchbinder, B.R., Weisskoff, R.M., Cohen, M.S., Vevea, J.M., Brady, T.J., Rosen, B.R., 1991. Functional mapping of the human visual cortex by magnetic resonance imaging. Science 254, 716–719.
Blinder, P., Tsai, P.S., Kaufhold, J.P., Knutsen, P.M., Suhl, H., Kleinfeld, D., 2013. The cortical angiome: an interconnected vascular network with noncolumnar patterns of blood flow. Nat. Neurosci. 16, 889–897.
Blockley, N.P., Driver, I.D., Fisher, J.A., Francis, S.T., Gowland, P.A., 2012. Measuring venous blood volume changes during activation using hyperoxia. Neuroimage 59, 3266–3274.
Blockley, N.P., Griffeth, V.E., Germuska, M.A., Bulte, D.P., Buxton, R.B., 2013a. An analysis of the use of hyperoxia for measuring venous cerebral blood volume: comparison of the existing method with a new analysis approach. Neuroimage 72, 33–40.
Blockley, N.P., Griffeth, V.E., Simon, A.B., Buxton, R.B., 2013b. A review of calibrated blood oxygenation level-dependent (BOLD) methods for the measurement of task-induced changes in brain oxygen metabolism. NMR Biomed. 26, 987–1003.
Brookes, M.J., Morris, P.G., Gowland, P.A., Francis, S.T., 2007. Noninvasive measurement of arterial cerebral blood volume using Look-Locker EPI and arterial spin labeling. Magn. Reson. Med. 58, 41–54.
Brueckl, C., Kaestle, S., Kerem, A., Habazettl, H., Krombach, F., Kuppe, H., Kuebler, W.M., 2006. Hyperoxia-induced reactive oxygen species formation in pulmonary capillary endothelial cells in situ. Am. J. Respir. Cell Mol. Biol. 34, 453–463.
Bulte, D., Chiarelli, P., Wise, R., Jezzard, P., 2007a. Measurement of cerebral blood volume in humans using hyperoxic MRI contrast. J. Magn. Reson. Imag. 26, 894–899.
Bulte, D.P., Chiarelli, P.A., Wise, R.G., Jezzard, P., 2007b. Cerebral perfusion response to hyperoxia. J. Cerebr. Blood Flow Metabol. 27, 69–75.
Bulte, D.P., Drescher, K., Jezzard, P., 2009. Comparison of hypercapnia-based calibration techniques for measurement of cerebral oxygen metabolism with MRI. Magn. Reson. Med. 61, 391–398.
Buxton, R.B., Frank, L.R., 1997. A model for the coupling between cerebral blood flow and oxygen metabolism during neural stimulation. J. Cerebr. Blood Flow Metabol. 17, 64–72.
Buxton, R.B., Wong, E.C., Frank, L.R., 1998. Dynamics of blood flow and oxygenation changes during brain activation: the balloon model. Magn. Reson. Med. 39, 855–864.
Cepeda-Prado, E., Popp, S., Khan, U., Stefanov, D., Rodriguez, J., Menalled, L.B., Dow-Edwards, D., Small, S.A., Moreno, H., 2012. R6/2 Huntington's disease mice develop early and progressive abnormal brain metabolism and seizures. J. Neurosci. 32, 6456–6467.
Cha, S., Knopp, E.A., Johnson, G., Wetzel, S.G., Litt, A.W., Zagzag, D., 2002. Intracranial mass lesions: dynamic contrast-enhanced susceptibility-weighted echo-planar perfusion MR imaging. Radiology 223, 11–29.
Chappell, M.A., MacIntosh, B.J., Donahue, M.J., Gunther, M., Jezzard, P., Woolrich, M.W., 2010. Separation of macrovascular signal in multi-inversion time arterial spin labelling MRI. Magn. Reson. Med. 63, 1357–1365.
Chen, J.J., Pike, G.B., 2009a. BOLD-specific cerebral blood volume and blood flow changes during neuronal activation in humans. NMR Biomed. 22, 1054–1062.
Chen, J.J., Pike, G.B., 2009b. Origins of the BOLD post-stimulus undershoot. Neuroimage 46, 559–568.
Chen, J.J., Pike, G.B., 2010. MRI measurement of the BOLD-specific flow-volume relationship during hypercapnia and hypocapnia in humans. Neuroimage 53, 383–391.
Christen, T., Lemasson, B., Pannetier, N., Farion, R., Remy, C., Zaharchuk, G., Barbier, E.L., 2012. Is T2* enough to assess oxygenation? Quantitative blood oxygen level-dependent analysis in brain tumor. Radiology 262, 495–502.
Christen, T., Lemasson, B., Pannetier, N., Farion, R., Segebarth, C., Remy, C., Barbier, E.L., 2011. Evaluation of a quantitative blood oxygenation level-dependent (qBOLD) approach to map local blood oxygen saturation. NMR Biomed. 24, 393–403.
Christen, T., Pannetier, N.A., Ni, W.W., Qiu, D., Moseley, M.E., Schuff, N., Zaharchuk, G., 2014. MR vascular fingerprinting: a new approach to compute cerebral blood volume, mean vessel radius, and oxygenation maps in the human brain. Neuroimage 89, 262–270.
Christiansen, J., Douglas, C.G., Haldane, J.S., 1914. The absorption and dissociation of carbon dioxide by human blood. J. Physiol. 48, 244–271.
Corder, E.H., Saunders, A.M., Strittmatter, W.J., Schmechel, D.E., Gaskell, P.C., Small, G.W., Roses, A.D., Haines, J.L., Pericak-Vance, M.A., 1993. Gene dose of apolipoprotein E type 4 allele and the risk of Alzheimer's disease in late onset families. Science 261, 921–923.
D'Arceuil, H., Coimbra, A., Triano, P., Dougherty, M., Mello, J., Moseley, M., Glover, G., Lansberg, M., Blankenberg, F., 2013. Ferumoxytol enhanced resting state fMRI and relative cerebral blood volume mapping in normal human brain. Neuroimage 83, 200–209.
Dai, W., Garcia, D., de Bazelaire, C., Alsop, D.C., 2008. Continuous flow-driven inversion for arterial spin labeling using pulsed radio frequency and gradient fields. Magn. Reson. Med. 60, 1488–1497.
Davis, T.L., Kwong, K.K., Weisskoff, R.M., Rosen, B.R., 1998. Calibrated functional MRI: mapping the dynamics of oxidative metabolism. Proc. Natl. Acad. Sci. U. S. A. 95, 1834–1839.
Derdeyn, C.P., Videen, T.O., Yundt, K.D., Fritsch, S.M., Carpenter, D.A., Grubb, R.L., Powers, W.J., 2002. Variability of cerebral blood volume and oxygen extraction: stages of cerebral haemodynamic impairment revisited. Brain 125, 595–607.
Detre, J.A., Leigh, J.S., Williams, D.S., Koretsky, A.P., 1992. Perfusion imaging. Magn. Reson. Med. 23, 37–45.

Dickson, J.D., Ash, T.W., Williams, G.B., Sukstanskii, A.L., Ansorge, R.E., Yablonskiy, D.A., 2011. Quantitative phenomenological model of the BOLD contrast mechanism. J. Magn. Reson. 212, 17–25.
Diringer, M.N., Aiyagari, V., Zazulia, A.R., Videen, T.O., Powers, W.J., 2007. Effect of hyperoxia on cerebral metabolic rate for oxygen measured using positron emission tomography in patients with acute severe head injury. J. Neurosurg. 106, 526–529.
Donahue, M.J., Achten, E., Cogswell, P.M., De Leeuw, F.E., Derdeyn, C.P., Dijkhuizen, R.M., Fan, A.P., Ghaznawi, R., Heit, J.J., Ikram, M.A., Jezzard, P., Jordan, L.C., Jouvent, E., Knutsson, L., Leigh, R., Liebeskind, D.S., Lin, W., Okell, T.W., Qureshi, A.I., Stagg, C.J., van Osch, M.J., van Zijl, P.C., Watchmaker, J.M., Wintermark, M., Wu, O., Zaharchuk, G., Zhou, J., Hendrikse, J., 2017. Consensus statement on current and emerging methods for the diagnosis and evaluation of cerebrovascular disease. J. Cerebr. Blood Flow Metabol. 271678X17721830.
Donahue, M.J., Dethrage, L.M., Faraco, C.C., Jordan, L.C., Clemmons, P., Singer, R., Mocco, J., Shyr, Y., Desai, A., O'Duffy, A., Riebau, D., Hermann, L., Connors, J., Kirshner, H., Strother, M.K., 2014. Routine clinical evaluation of cerebrovascular reserve capacity using carbogen in patients with intracranial stenosis. Stroke 45, 2335–2341.
Donahue, M.J., MacIntosh, B.J., Sideso, E., Bright, M., Kennedy, J., Handa, A., Jezzard, P., 2009a. Absolute cerebral blood volume (CBV) quantification without contrast agents using inflow vascular-space-occupancy (iVASO) with dynamic subtraction. In: Proc. 17th Annual Meeting ISMRM, Hawaii, USA, p. 628.
Donahue, M.J., Sideso, E., MacIntosh, B.J., Kennedy, J., Handa, A., Jezzard, P., 2010. Absolute arterial cerebral blood volume quantification using inflow vascular-space-occupancy with dynamic subtraction magnetic resonance imaging. J. Cerebr. Blood Flow Metabol. 30, 1329–1342.
Donahue, M.J., Stevens, R.D., Hua, J., Huang, A.J., Pekar, J., van Zijl, P.C.M., 2009b. Cerebral blood flow (CBF) and cerebral blood volume (CBV) coupling differs during neuronal and vascular tasks. In: Proc. 17th Annual Meeting ISMRM, Hawaii, USA, p. 513.
Drouin-Ouellet, J., Sawiak, S.J., Cisbani, G., Lagace, M., Kuan, W.L., Saint-Pierre, M., Dury, R.J., Alata, W., St-Amour, I., Mason, S.L., Calon, F., Lacroix, S., Gowland, P.A., Francis, S.T., Barker, R.A., Cicchetti, F., 2015. Cerebrovascular and blood-brain barrier impairments in Huntington's disease: potential implications for its pathophysiology. Ann. Neurol. 78, 160–177.
Duhamel, G., de Bazelaire, C., Alsop, D.C., 2003. Evaluation of systematic quantification errors in velocity-selective arterial spin labeling of the brain. Magn. Reson. Med. 50, 145–153.
Duong, T.Q., Kim, S.G., 2000. In vivo MR measurements of regional arterial and venous blood volume fractions in intact rat brain. Magn. Reson. Med. 43, 393–402.
Folkman, J., 1995. Angiogenesis in cancer, vascular, rheumatoid and other disease. Nat. Med. 1, 27–31.
Franciosi, S., Ryu, J.K., Shim, Y., Hill, A., Connolly, C., Hayden, M.R., McLarnon, J.G., Leavitt, B.R., 2012. Age-dependent neurovascular abnormalities and altered microglial morphology in the YAC128 mouse model of Huntington disease. Neurobiol. Dis. 45, 438–449.
Francis, S.T., Bowtell, R., Gowland, P.A., 2008. Modeling and optimization of Look-Locker spin labeling for measuring perfusion and transit time changes in activation studies taking into account arterial blood volume. Magn. Reson. Med. 59, 316–325.
Fujita, N., 2001. Extravascular contribution of blood oxygenation level-dependent signal changes: a numerical analysis based on a vascular network model. Magn. Reson. Med. 46, 723–734.
Germuska, M., Bulte, D.P., 2014. MRI measurement of oxygen extraction fraction, mean vessel size and cerebral blood volume using serial hyperoxia and hypercapnia. Neuroimage 92, 132–142.
Gonzalez, R.G., Fischman, A.J., Guimaraes, A.R., Carr, C.A., Stern, C.E., Halpern, E.F., Growdon, J.H., Rosen, B.R., 1995. Functional MR in the evaluation of dementia: correlation of abnormal dynamic cerebral blood volume measurements with changes in cerebral metabolism on positron emission tomography with fludeoxyglucose F 18. AJNR Am J Neuroradiol 16, 1763–1770.
Griffeth, V.E., Buxton, R.B., 2011. A theoretical framework for estimating cerebral oxygen metabolism changes using the calibrated-BOLD method: modeling the effects of blood volume distribution, hematocrit, oxygen extraction fraction, and tissue signal properties on the BOLD signal. Neuroimage 58, 198–212.
Group, T.H.s.D.C.R., 1993. A novel gene containing a trinucleotide repeat that is expanded and unstable on Huntington's disease chromosomes. Cell 72, 971–983.
Grubb Jr., R.L., Raichle, M.E., Eichling, J.O., Ter-Pogossian, M.M., 1974. The effects of changes in PaCO2 on cerebral blood volume, blood flow, and vascular mean transit time. Stroke 5, 630–639.
Hales, P.W., Phipps, K.P., Kaur, R., Clark, C.A., 2013. A two-stage model for in vivo assessment of brain tumor perfusion and abnormal vascular structure using arterial spin labeling. PLoS One 8 e75717.
Hansen-Smith, F., Egginton, S., Zhou, A.L., Hudlicka, O., 2001. Growth of arterioles precedes that of capillaries in stretch-induced angiogenesis in skeletal muscle. Microvasc. Res. 62, 1–14.
Harper, S.L., Bohlen, H.G., 1984. Microvascular adaptation in the cerebral cortex of adult spontaneously hypertensive rats. Hypertension 6, 408–419.
Harris, G.J., Lewis, R.F., Satlin, A., English, C.D., Scott, T.M., Yurgelun-Todd, D.A., Renshaw, P.F., 1996. Dynamic susceptibility contrast MRI of regional cerebral blood volume in Alzheimer's disease. Am. J. Psychiatr. 153, 721–724.
Havlicek, M., Ivanov, D., Poser, B.A., Uludag, K., 2017. Echo-time dependence of the BOLD response transients - a window into brain functional physiology. Neuroimage 159, 355–370.
He, X., Yablonskiy, D.A., 2007. Quantitative BOLD: mapping of human cerebral deoxygenated blood volume and oxygen extraction fraction: default state. Magn. Reson. Med. 57, 115–126.
He, X., Zhu, M., Yablonskiy, D.A., 2008. Validation of oxygen extraction fraction measurement by qBOLD technique. Magn. Reson. Med. 60, 882–888.
Heijtel, D.F., Petersen, E.T., Mutsaerts, H.J., Bakker, E., Schober, P., Stevens, M.F., van Berckel, B.N., Majoie, C.B., Booij, J., van Osch, M.J., van Bavel, E.T., Boellaard, R., Lammertsma, A.A., Nederveen, A.J., 2016. Quantitative agreement between [(15)O] H2O PET and model free QUASAR MRI-derived cerebral blood flow and arterial blood volume. NMR Biomed. 29, 519–526.
Heit, J.J., Wintermark, M., 2016. Perfusion computed tomography for the evaluation of acute ischemic stroke: strengths and pitfalls. Stroke 47, 1153–1158.
Hendrikse, J., Petersen, E.T., van Laar, P.J., Golay, X., 2008. Cerebral border zones between distal end branches of intracranial arteries: MR imaging. Radiology 246, 572–580.
Hillman, E.M., Devor, A., Bouchard, M.B., Dunn, A.K., Krauss, G.W., Skoch, J., Bacskai, B.J., Dale, A.M., Boas, D.A., 2007. Depth-resolved optical imaging and microscopy of vascular compartment dynamics during somatosensory stimulation. Neuroimage 35, 89–104.
Hoge, R.D., Atkinson, J., Gill, B., Crelier, G.R., Marrett, S., Pike, G.B., 1999. Investigation of BOLD signal dependence on cerebral blood flow and oxygen consumption: the deoxyhemoglobin dilution model. Magn. Reson. Med. 42, 849–863.
Hua, J., Brandt, A.S., Lee, S., Blair, N.I., Wu, Y., Lui, S., Patel, J., Faria, A.V., Lim, I.A., Unschuld, P.G., Pekar, J.J., van Zijl, P.C., Ross, C.A., Margolis, R.L., 2016a. Abnormal grey matter arteriolar cerebral blood volume in schizophrenia measured with 3D inflow-based vascular-space-occupancy MRI at 7T. Schizophr. Bull. 43, 620–632.
Hua, J., Donahue, M.J., Zhao, J.M., Grgac, K., Huang, A.J., Zhou, J., van Zijl, P.C., 2009a. Magnetization transfer enhanced vascular-space-occupancy (MT-VASO) functional MRI. Magn. Reson. Med. 61, 944–951.
Hua, J., Lee, S., Blair, N.I.S., Wyss, M., Schreiner, S., Steininger, S.C., Leh, S., Nitsch, R., Pruessmann, K.P., van zijl, P.C.M., Albert, M., Hock, C., Unschuld, P.G., 2016b. Abnormal grey matter arteriolar cerebral blood volume and its association with the presence of E4 allele of the apolipoprotein E (APOE) gene in elderly subjects at risk for Alzheimer's disease (AD). In: Proc. 24th Annual Meeting ISMRM, Singapore, p. 4030.
Hua, J., Qin, Q., Donahue, M.J., Zhou, J., Pekar, J., van Zijl, P.C.M., 2009b. Functional MRI using arteriolar cerebral blood volume changes. In: Proc. 17th Annual Meeting ISMRM, Hawaii, USA, p. 12.
Hua, J., Qin, Q., Donahue, M.J., Zhou, J., Pekar, J.J., van Zijl, P.C., 2011a. Inflow-based vascular-space-occupancy (iVASO) MRI. Magn. Reson. Med. 66, 40–56.
Hua, J., Qin, Q., Pekar, J., van Zijl, P.C.M., 2009c. Measuring absolute arteriolar cerebral blood volume (CBVa) in human brain gray matter (GM) without contrast agent. In: Proc. 17th Annual Meeting ISMRM, Hawaii, USA, p. 5314.
Hua, J., Qin, Q., Pekar, J.J., Zijl, P.C., 2011b. Measurement of absolute arterial cerebral blood volume in human brain without using a contrast agent. NMR Biomed. 24, 1313–1325.
Hua, J., Stevens, R., Donahue, M.J., Huang, A.J., Pekar, J., van Zijl, P.C.M., 2010. Cerebral blood volume changes in arterial and post-arterial compartments and their relationship with cerebral blood flow alteration during brief breath-holding and visual stimulation in human brain. In: Proc. 18th Annual Meeting ISMRM, Stockholm, Sweden, p. 1127.
Hua, J., Stevens, R.D., Huang, A.J., Pekar, J.J., van Zijl, P.C., 2011c. Physiological origin for the BOLD poststimulus undershoot in human brain: vascular compliance versus oxygen metabolism. J. Cerebr. Blood Flow Metabol. 31, 1599–1611.
Hua, J., Unschuld, P.G., Margolis, R.L., van Zijl, P.C., Ross, C.A., 2014. Elevated arteriolar cerebral blood volume in prodromal Huntington's disease. Mov. Disord. 29, 396–401.
Hua, J., Wyss, M., van Bergen, J.M., Schreiner, S., Steininger, S.C., Gietl, A., Buck, A., Nitsch, R., Pruessmann, K.P., Lu, H., van Zijl, P.C.M., Albert, M., Hock, C., Unschuld, P.G., 2017. Synergistic effect of ß-amyloid and microvascular abnormality on longitudinal cognitive decline in elderly subjects at risk for Alzheimer's disease (AD). In: Proc. 25th Annual Meeting ISMRM, Hawaii, HI, USA, p. 2365.
Huber, L., Goense, J., Kennerley, A.J., Ivanov, D., Krieger, S.N., Lepsien, J., Trampel, R., Turner, R., Moller, H.E., 2014. Investigation of the neurovascular coupling in positive and negative BOLD responses in human brain at 7 T. Neuroimage 97, 349–362.
Huber, L., Handwerker, D.A., Jangraw, D.C., Chen, G., Hall, A., Stuber, C., Gonzalez-Castillo, J., Ivanov, D., Marrett, S., Guidi, M., Goense, J., Poser, B.A., Bandettini, P.A., 2017a. High-resolution CBV-fMRI allows mapping of laminar activity and connectivity of cortical input and output in human M1. Neuron 96, 1253–1263 e1257.
Huber, L., Uludag, K., Moller, H.E., 2017b. Non-BOLD contrast for laminar fMRI in humans: CBF, CBV, and CMRO2. Neuroimage. https://doi.org/10.1016/j.neuroimage.2017.07.041.
Iadecola, C., 2004. Neurovascular regulation in the normal brain and in Alzheimer's disease. Nat. Rev. Neurosci. 5, 347–360.
Iadecola, C., Nedergaard, M., 2007. Glial regulation of the cerebral microvasculature. Nat. Neurosci. 10, 1369–1376.
Iadecola, C., Yang, G., Ebner, T.J., Chen, G., 1997. Local and propagated vascular responses evoked by focal synaptic activity in cerebellar cortex. J. Neurophysiol. 78, 651–659.
Iliff, J.J., Wang, M., Liao, Y., Plogg, B.A., Peng, W., Gundersen, G.A., Benveniste, H., Vates, G.E., Deane, R., Goldman, S.A., Nagelhus, E.A., Nedergaard, M., 2012. A paravascular pathway facilitates CSF flow through the brain parenchyma and the clearance of interstitial solutes, including amyloid beta. Sci. Transl. Med. 4, 147ra111.
Iscoe, S., Fisher, J.A., 2005. Hyperoxia-induced hypocapnia: an underappreciated risk. Chest 128, 430–433.
Ito, H., Ibaraki, M., Kanno, I., Fukuda, H., Miura, S., 2005. Changes in the arterial fraction of human cerebral blood volume during hypercapnia and hypocapnia measured by positron emission tomography. J. Cerebr. Blood Flow Metabol. 25, 852–857.

Ito, H., Kanno, I., Iida, H., Hatazawa, J., Shimosegawa, E., Tamura, H., Okudera, T., 2001. Arterial fraction of cerebral blood volume in humans measured by positron emission tomography. Ann. Nucl. Med. 15, 111–116.
Iturria-Medina, Y., Sotero, R.C., Toussaint, P.J., Mateos-Perez, J.M., Evans, A.C., Alzheimer's Disease Neuroimaging, I, 2016. Early role of vascular dysregulation on late-onset Alzheimer's disease based on multifactorial data-driven analysis. Nat. Commun. 7, 11934.
Jahanian, H., Peltier, S., Noll, D.C., Hernandez Garcia, L., 2015. Arterial cerebral blood volume-weighted functional MRI using pseudocontinuous arterial spin tagging (AVAST). Magn. Reson. Med. 73, 1053–1064.
Jensen, F.B., 2004. Red blood cell pH, the Bohr effect, and other oxygenation-linked phenomena in blood O2 and CO2 transport. Acta Physiol. Scand. 182, 215–227.
Jin, T., Kim, S.G., 2008. Improved cortical-layer specificity of vascular space occupancy fMRI with slab inversion relative to spin-echo BOLD at 9.4 T. Neuroimage 40, 59–67.
Jochimsen, T.H., Ivanov, D., Ott, D.V., Heinke, W., Turner, R., Moller, H.E., Reichenbach, J.R., 2010. Whole-brain mapping of venous vessel size in humans using the hypercapnia-induced BOLD effect. Neuroimage 51, 765–774.
Johnston, A.J., Steiner, L.A., Balestreri, M., Gupta, A.K., Menon, D.K., 2003a. Hyperoxia and the cerebral hemodynamic responses to moderate hyperventilation. Acta Anaesthesiol. Scand. 47, 391–396.
Johnston, A.J., Steiner, L.A., Gupta, A.K., Menon, D.K., 2003b. Cerebral oxygen vasoreactivity and cerebral tissue oxygen reactivity. Br. J. Anaesth. 90, 774–786.
Kety, S.S., Schmidt, C.F., 1948. The nitrous oxide method for the quantitative determination of cerebral blood flow in man: theory, procedure and normal values. J. Clin. Invest. 27, 476–483.
Kida, I., Rothman, D.L., Hyder, F., 2007. Dynamics of changes in blood flow, volume, and oxygenation: implications for dynamic functional magnetic resonance imaging calibration. J. Cerebr. Blood Flow Metabol. 27, 690–696.
Kim, K.H., Choi, S.H., Park, S.H., 2016. Feasibility of quantifying arterial cerebral blood volume using multiphase alternate ascending/descending directional navigation (ALADDIN). PLoS One 11 e0156687.
Kim, S.G., Rostrup, E., Larsson, H.B., Ogawa, S., Paulson, O.B., 1999. Determination of relative CMRO2 from CBF and BOLD changes: significant increase of oxygen consumption rate during visual stimulation. Magn. Reson. Med. 41, 1152–1161.
Kim, T., Hendrich, K., Kim, S.G., 2008. Functional MRI with magnetization transfer effects: determination of BOLD and arterial blood volume changes. Magn. Reson. Med. 60, 1518–1523.
Kim, T., Hendrich, K.S., Masamoto, K., Kim, S.G., 2007. Arterial versus total blood volume changes during neural activity-induced cerebral blood flow change: implication for BOLD fMRI. J. Cerebr. Blood Flow Metabol. 27, 1235–1247.
Kim, T., Kim, S.G., 2005. Quantification of cerebral arterial blood volume and cerebral blood flow using MRI with modulation of tissue and vessel (MOTIVE) signals. Magn. Reson. Med. 54, 333–342.
Kim, T., Kim, S.G., 2006. Quantification of cerebral arterial blood volume using arterial spin labeling with intravoxel incoherent motion-sensitive gradients. Magn. Reson. Med. 55, 1047–1057.
Kim, T., Kim, S.G., 2010. Cortical layer-dependent arterial blood volume changes: improved spatial specificity relative to BOLD fMRI. Neuroimage 49, 1340–1349.
Kim, T., Kim, S.G., 2011. Temporal dynamics and spatial specificity of arterial and venous blood volume changes during visual stimulation: implication for BOLD quantification. J. Cerebr. Blood Flow Metabol. 31, 1211–1222.
Kim, T., Richard Jennings, J., Kim, S.G., 2014. Regional cerebral blood flow and arterial blood volume and their reactivity to hypercapnia in hypertensive and normotensive rats. J. Cerebr. Blood Flow Metabol. 34, 408–414.
Kim, T., Shin, W., Zhao, T., Beall, E.B., Lowe, M.J., Bae, K.T., 2013. Whole brain perfusion measurements using arterial spin labeling with multiband acquisition. Magn. Reson. Med. 70, 1653–1661.
Kiselev, V.G., Posse, S., 1999. Analytical model of susceptibility-induced MR signal dephasing: effect of diffusion in a microvascular network. Magn. Reson. Med. 41, 499–509.
Kisler, K., Nelson, A.R., Montagne, A., Zlokovic, B.V., 2017. Cerebral blood flow regulation and neurovascular dysfunction in Alzheimer disease. Nat. Rev. Neurosci. 18, 419–434.
Kobari, M., Gotoh, F., Fukuuchi, Y., Tanaka, K., Suzuki, N., Uematsu, D., 1984. Blood flow velocity in the pial arteries of cats, with particular reference to the vessel diameter. J. Cerebr. Blood Flow Metabol. 4, 110–114.
Koenig, M., Klotz, E., Luka, B., Venderink, D.J., Spittler, J.F., Heuser, L., 1998. Perfusion CT of the brain: diagnostic approach for early detection of ischemic stroke. Radiology 209, 85–93.
Kreczmanski, P., Heinsen, H., Mantua, V., Woltersdorf, F., Masson, T., Ulfig, N., Schmidt-Kastner, R., Korr, H., Steinbusch, H.W., Hof, P.R., Schmitz, C., 2009. Microvessel length density, total length, and length per neuron in five subcortical regions in schizophrenia. Acta Neuropathol. 117, 409–421.
Kreczmanski, P., Schmidt-Kastner, R., Heinsen, H., Steinbusch, H.W., Hof, P.R., Schmitz, C., 2005. Stereological studies of capillary length density in the frontal cortex of schizophrenics. Acta Neuropathol. 109, 510–518.
Krieger, S.N., Streicher, M.N., Trampel, R., Turner, R., 2012. Cerebral blood volume changes during brain activation. J. Cerebr. Blood Flow Metabol. 32, 1618–1631.
Kuschinsky, W., Mraovitch, S., Sercombe, R., 1996. Regulation of Cerebral Blood Flow: an Overview. Neurophysiological Basis of Cerebral Blood Flow Control: an Introduction. Johns Libbey & Company Ltd., London, p. 245.
Lacalle-Aurioles, M., Mateos-Perez, J.M., Guzman-De-Villoria, J.A., Olazaran, J., Cruz-Orduna, I., Aleman-Gomez, Y., Martino, M.E., Desco, M., 2014. Cerebral blood flow is an earlier indicator of perfusion abnormalities than cerebral blood volume in Alzheimer's disease. J. Cerebr. Blood Flow Metabol. 34, 654–659.
Laurent, S., Boutouyrie, P., Lacolley, P., 2005. Structural and genetic bases of arterial stiffness. Hypertension 45, 1050–1055.
Law, M., Yang, S., Babb, J.S., Knopp, E.A., Golfinos, J.G., Zagzag, D.G.J., 2004. Comparison of cerebral blood volume and vascular permeability from dynamic susceptibility contrast-enhanced perfusion MR imaging with glioma grade. Am. J. Neuroradiol. 25, 746–755.
Le Bihan, D., Breton, E., Lallemand, D., Aubin, M.L., Vignaud, J., Laval-Jeantet, M., 1988. Separation of diffusion and perfusion in intravoxel incoherent motion MR imaging. Radiology 168, 497–505.
Lee, S.P., Duong, T.Q., Yang, G., Iadecola, C., Kim, S.G., 2001. Relative changes of cerebral arterial and venous blood volumes during increased cerebral blood flow: implications for BOLD fMRI. Magn. Reson. Med. 45, 791–800.
Lee, Y., Kim, T., 2017. Assessment of hypertensive cerebrovascular alterations with multiband Look-Locker arterial spin labeling. J. Magn. Reson. Imag. https://doi.org/10.1002/jmri.25812.
Leeuwis, A.E., Benedictus, M.R., Kuijer, J.P.A., Binnewijzend, M.A.A., Hooghiemstra, A.M., Verfaillie, S.C.J., Koene, T., Scheltens, P., Barkhof, F., Prins, N.D., van der Flier, W.M., 2017. Lower cerebral blood flow is associated with impairment in multiple cognitive domains in Alzheimer's disease. Alzheimers Dement 13, 531–540.
Leite, F.P., Tsao, D., Vanduffel, W., Fize, D., Sasaki, Y., Wald, L.L., Dale, A.M., Kwong, K.K., Orban, G.A., Rosen, B.R., Tootell, R.B., Mandeville, J.B., 2002. Repeated fMRI using iron oxide contrast agent in awake, behaving macaques at 3 Tesla. Neuroimage 16, 283–294.
Lin, C., Huang, C., Lin, M., Hsu, Y., Tsai, C., Chen, H., Chern, Y., Chang, C., 2010. Magnetic resonance microscopic angiography visualization of abnormal microvasculature in a transgenic mouse model of Huntington's disease. In: Proc. 18th Annual Meeting ISMRM, Stockholm, Sweden, p. 462.
Lin, W., Powers, W.J., 2017. Oxygen metabolism in acute ischemic stroke. J. Cerebr. Blood Flow Metabol. 271678X17722095.
Liu, D., Xu, F., Lin, D.D., van Zijl, P.C.M., Qin, Q., 2017a. Quantitative measurement of cerebral blood volume using velocity-selective pulse trains. Magn. Reson. Med. 77, 92–101.
Liu, P., Welch, B.G., Li, Y., Gu, H., King, D., Yang, Y., Pinho, M., Lu, H., 2017b. Multiparametric imaging of brain hemodynamics and function using gas-inhalation MRI. Neuroimage 146, 715–723.
Lu, H., Golay, X., Pekar, J.J., van Zijl, P.C., 2003. Functional magnetic resonance imaging based on changes in vascular space occupancy. Magn. Reson. Med. 50, 263–274.
Lu, H., Hua, J., van Zijl, P.C., 2013. Noninvasive functional imaging of cerebral blood volume with vascular-space-occupancy (VASO) MRI. NMR Biomed. 26, 932–948.
Lu, H., Law, M., Johnson, G., Ge, Y., van Zijl, P.C., Helpern, J.A., 2005. Novel approach to the measurement of absolute cerebral blood volume using vascular-space-occupancy magnetic resonance imaging. Magn. Reson. Med. 54, 1403.
Lu, H., van Zijl, P.C., 2012. A review of the development of Vascular-Space-Occupancy (VASO) fMRI. Neuroimage 62, 736–742.
Lu, H., Xu, F., Grgac, K., Liu, P., Qin, Q., van Zijl, P., 2012. Calibration and validation of TRUST MRI for the estimation of cerebral blood oxygenation. Magn. Reson. Med. 67, 42–49.
Lucotte, B.M., Powell, C., Knutson, J.R., Combs, C.A., Malide, D., Yu, Z.X., Knepper, M., Patel, K.D., Pielach, A., Johnson, E., Borysova, L., Dora, K.A., Balaban, R.S., 2017. Direct visualization of the arterial wall water permeability barrier using CARS microscopy. Proc. Natl. Acad. Sci. U. S. A. 114, 4805–4810.
Mandeville, J.B., Marota, J.J., Ayata, C., Zaharchuk, G., Moskowitz, M.A., Rosen, B.R., Weisskoff, R.M., 1999. Evidence of a cerebrovascular postarteriole windkessel with delayed compliance. J. Cerebr. Blood Flow Metabol. 19, 679–689.
Mandeville, J.B., Marota, J.J., Kosofsky, B.E., Keltner, J.R., Weissleder, R., Rosen, B.R., Weisskoff, R.M., 1998. Dynamic functional imaging of relative cerebral blood volume during rat forepaw stimulation. Magn. Reson. Med. 39, 615–624.
Mark, C.I., Pike, G.B., 2012. Indication of BOLD-specific venous flow-volume changes from precisely controlled hyperoxic vs. hypercapnic calibration. J. Cerebr. Blood Flow Metabol. 32, 709–719.
Mchedlishvili, G., 1986. Arterial Behavior and Blood Circulation in the Brain. Plenum Press, New York.
Mchedlishvili, G.I., Baramidze, D.G., Nicolaishvili, L.S., Mamisashvili, V.A., 1974-75. Vascular mechanisms responsible for microcirculation of the cerebral cortex. Biochem. Exp. Biol. 11, 113–129.
Meng, Y., Wang, P., Kim, S.G., 2012. Simultaneous measurement of cerebral blood flow and transit time with turbo dynamic arterial spin labeling (Turbo-DASL): application to functional studies. Magn. Reson. Med. 68, 762–771.
Moseley, M.E., Chew, W.M., White, D.L., Kucharczyk, J., Litt, L., Derugin, N., Dupon, J., Brasch, R.C., Norman, D., 1992. Hypercarbia-induced changes in cerebral blood volume in the cat: a 1H MRI and intravascular contrast agent study. Magn. Reson. Med. 23, 21–30.
Mueser, K.T., McGurk, S.R., 2004. Schizophrenia. Lancet 363, 2063–2072.
Neil, J.J., Ackerman, J.J.H., 1992. Detection of pseudodiffusion in rat-brain following blood substitution with perfluorocarbon. J. Magn. Reson. 97, 194–201.
Niatsetskaya, Z., Basso, M., Speer, R.E., McConoughey, S.J., Coppola, G., Ma, T.C., Ratan, R.R., 2010. HIF prolyl hydroxylase inhibitors prevent neuronal death induced by mitochondrial toxins: therapeutic implications for Huntington's disease and Alzheimer's disease. Antioxidants Redox Signal. 12, 435–443.
Nielsen, R.B., Egefjord, L., Angleys, H., Mouridsen, K., Gejl, M., Moller, A., Brock, B., Braendgaard, H., Gottrup, H., Rungby, J., Eskildsen, S.F., Ostergaard, L., 2017. Capillary dysfunction is associated with symptom severity and neurodegeneration in Alzheimer's disease. Alzheimers Dement 13, 1143–1153.
Ogawa, S., Menon, R.S., Tank, D.W., Kim, S.G., Merkle, H., Ellermann, J.M., Ugurbil, K., 1993. Functional brain mapping by blood oxygenation level-dependent contrast

magnetic resonance imaging. A comparison of signal characteristics with a biophysical model. Biophys. J. 64, 803–812.
Ostergaard, L., Aamand, R., Gutierrez-Jimenez, E., Ho, Y.C., Blicher, J.U., Madsen, S.M., Nagenthiraja, K., Dalby, R.B., Drasbek, K.R., Moller, A., Braendgaard, H., Mouridsen, K., Jespersen, S.N., Jensen, M.S., West, M.J., 2013. The capillary dysfunction hypothesis of Alzheimer's disease. Neurobiol. Aging 34, 1018–1031.
Ostergaard, L., Sorensen, A.G., Kwong, K.K., Weisskoff, R.M., Gyldensted, C., Rosen, B.R., 1996a. High resolution measurement of cerebral blood flow using intravascular tracer bolus passages. Part II: experimental comparison and preliminary results. Magn. Reson. Med. 36, 726–736.
Ostergaard, L., Weisskoff, R.M., Chesler, D.A., Gyldensted, C., Rosen, B.R., 1996b. High resolution measurement of cerebral blood flow using intravascular tracer bolus passages. Part I: mathematical approach and statistical analysis. Magn. Reson. Med. 36, 715–725.
Pan, Y., You, J., Volkow, N.D., Park, K., Du, C., 2014. Ultrasensitive detection of 3D cerebral microvascular network dynamics in vivo. Neuroimage 103, 492–501.
Paulsen, J.S., Nopoulos, P.C., Aylward, E., Ross, C.A., Johnson, H., Magnotta, V.A., Juhl, A., Pierson, R.K., Mills, J., Langbehn, D., Nance, M., 2010. Striatal and white matter predictors of estimated diagnosis for Huntington disease. Brain Res. Bull. 82, 201–207.
Peruzzo, D., Rambaldelli, G., Bertoldo, A., Bellani, M., Cerini, R., Silvia, M., Pozzi Mucelli, R., Tansella, M., Brambilla, P., 2011. The impact of schizophrenia on frontal perfusion parameters: a DSC-MRI study. J. Neural. Transm. 118, 563–570.
Petersen, E.T., Lim, T., Golay, X., 2006. Model-free arterial spin labeling quantification approach for perfusion MRI. Magn. Reson. Med. 55, 219.
Petersen, E.T., Mouridsen, K., Golay, X., 2010. The QUASAR reproducibility study, Part II: results from a multi-center Arterial Spin Labeling test-retest study. Neuroimage 49, 104–113.
Piechnik, S.K., Chiarelli, P.A., Jezzard, P., 2008. Modelling vascular reactivity to investigate the basis of the relationship between cerebral blood volume and flow under CO2 manipulation. Neuroimage 39, 107–118.
Pires, P.W., Dams Ramos, C.M., Matin, N., Dorrance, A.M., 2013. The effects of hypertension on the cerebral circulation. Am. J. Physiol. Heart Circ. Physiol. 304, H1598–H1614.
Poulin, M.J., Liang, P.J., Robbins, P.A., 1998. Fast and slow components of cerebral blood flow response to step decreases in end-tidal PCO2 in humans. J. Appl. Physiol. 85, 388–397.
Qiu, D., Zaharchuk, G., Christen, T., Ni, W.W., Moseley, M.E., 2012. Contrast-enhanced functional blood volume imaging (CE-fBVI): enhanced sensitivity for brain activation in humans using the ultrasmall superparamagnetic iron oxide agent ferumoxytol. Neuroimage 62, 1726–1731.
Raichle, M.E., 1983. Positron emission tomography. Annu. Rev. Neurosci. 6, 249–267.
Rane, S., Grabowski, T., Gore, J., Hua, J., Donahue, M.J., 2017. Multi-slice extension of IVASO for absolute cerebral blood volume mapping using a 3D GRASE readout. In: Proc. 25th Annual Meeting ISMRM, Hawaii, HI, USA, p. 3847.
Rane, S., Talati, P., Donahue, M.J., Heckers, S., 2016. Inflow-vascular space occupancy (iVASO) reproducibility in the hippocampus and cortex at different blood water nulling times. Magn. Reson. Med. 75, 2379–2387.
Richards, E.M., Fiskum, G., Rosenthal, R.E., Hopkins, I., McKenna, M.C., 2007. Hyperoxic reperfusion after global ischemia decreases hippocampal energy metabolism. Stroke 38, 1578–1584.
Rockswold, S.B., Rockswold, G.L., Zaun, D.A., Zhang, X., Cerra, C.E., Bergman, T.A., Liu, J., 2010. A prospective, randomized clinical trial to compare the effect of hyperbaric to normobaric hyperoxia on cerebral metabolism, intracranial pressure, and oxygen toxicity in severe traumatic brain injury. J. Neurosurg. 112, 1080–1094.
Ross, C.A., Tabrizi, S.J., 2011. Huntington's disease: from molecular pathogenesis to clinical treatment. Lancet Neurol. 10, 83–98.
Rostrup, E., Knudsen, G.M., Law, I., Holm, S., Larsson, H.B., Paulson, O.B., 2005. The relationship between cerebral blood flow and volume in humans. Neuroimage 24, 1–11.
Schaller, B., 2004. Physiology of cerebral venous blood flow: from experimental data in animals to normal function in humans. Brain Res Brain Res Rev 46, 243–260.
Schobel, S.A., Chaudhury, N.H., Khan, U.A., Paniagua, B., Styner, M.A., Asllani, I., Inbar, B.P., Corcoran, C.M., Lieberman, J.A., Moore, H., Small, S.A., 2013. Imaging patients with psychosis and a mouse model establishes a spreading pattern of hippocampal dysfunction and implicates glutamate as a driver. Neuron 78, 81–93.
Schobel, S.A., Lewandowski, N.M., Corcoran, C.M., Moore, H., Brown, T., Malaspina, D., Small, S.A., 2009. Differential targeting of the CA1 subfield of the hippocampal formation by schizophrenia and related psychotic disorders. Arch. Gen. Psychiatr. 66, 938–946.
Sedlacik, J., Reichenbach, J.R., 2010. Validation of quantitative estimation of tissue oxygen extraction fraction and deoxygenated blood volume fraction in phantom and in vivo experiments by using MRI. Magn. Reson. Med. 63, 910–921.
Setsompop, K., Gagoski, B.A., Polimeni, J.R., Witzel, T., Wedeen, V.J., Wald, L.L., 2012. Blipped-controlled aliasing in parallel imaging for simultaneous multislice echo planar imaging with reduced g-factor penalty. Magn. Reson. Med. 67, 1210–1224.
Sharan Jr., M.D.,J.M., Koehler, R.C., Traystman, R.J., Popel, A.S., 1989. A compartmental model for oxygen transport in brain microcirculation. Ann. Biomed. Eng. 17, 13–38.
Shen, Y., Pu, I.M., Ahearn, T., Clemence, M., Schwarzbauer, C., 2013. Quantification of venous vessel size in human brain in response to hypercapnia and hyperoxia using magnetic resonance imaging. Magn. Reson. Med. 69, 1541–1552.
Shen, Z., Lu, Z., Chhatbar, P.Y., O'Herron, P., Kara, P., 2012. An artery-specific fluorescent dye for studying neurovascular coupling. Nat Methods 9, 273–276.
Siero, J.C., Strother, M.K., Faraco, C.C., Hoogduin, H., Hendrikse, J., Donahue, M.J., 2015. In vivo quantification of hyperoxic arterial blood water T1. NMR Biomed. 28, 1518–1525.
Silva, A.C., Williams, D.S., Koretsky, A.P., 1997. Evidence for the exchange of arterial spin-labeled water with tissue water in rat brain from diffusion-sensitized measurements of perfusion. Magn. Reson. Med. 38, 232–237.
Spano, V.R., Mandell, D.M., Poublanc, J., Sam, K., Battisti-Charbonney, A., Pucci, O., Han, J.S., Crawley, A.P., Fisher, J.A., Mikulis, D.J., 2013. CO2 blood oxygen level-dependent MR mapping of cerebrovascular reserve in a clinical population: safety, tolerability, and technical feasibility. Radiology 266, 592–598.
Stefanovic, B., Pike, G.B., 2005. Venous refocusing for volume estimation: VERVE functional magnetic resonance imaging. Magn. Reson. Med. 53, 339–347.
Tabrizi, S.J., Langbehn, D.R., Leavitt, B.R., Roos, R.A., Durr, A., Craufurd, D., Kennard, C., Hicks, S.L., Fox, N.C., Scahill, R.I., Borowsky, B., Tobin, A.J., Rosas, H.D., Johnson, H., Reilmann, R., Landwehrmeyer, B., Stout, J.C., 2009. Biological and clinical manifestations of Huntington's disease in the longitudinal TRACK-HD study: cross-sectional analysis of baseline data. Lancet Neurol. 8, 791–801.
Takano, T., Tian, G.F., Peng, W., Lou, N., Libionka, W., Han, X., Nedergaard, M., 2006. Astrocyte-mediated control of cerebral blood flow. Nat. Neurosci. 9, 260–267.
Talati, P., Rane, S., Donahue, M.J., Heckers, S., 2016. Hippocampal arterial cerebral blood volume in early psychosis. Psychiatr. Res. 256, 21–25.
Talati, P., Rane, S., Kose, S., Blackford, J.U., Gore, J., Donahue, M.J., Heckers, S., 2014. Increased hippocampal CA1 cerebral blood volume in schizophrenia. Neuroimage Clin 5, 359–364.
Tamminga, C.A., Southcott, S., Sacco, C., Wagner, A.D., Ghose, S., 2012. Glutamate dysfunction in hippocampus: relevance of dentate gyrus and CA3 signaling. Schizophr. Bull. 38, 927–935.
Tang, C.C., Feigin, A., Ma, Y., Habeck, C., Paulsen, J.S., Leenders, K.L., Teune, L.K., van Oostrom, J.C., Guttman, M., Dhawan, V., Eidelberg, D., 2013. Metabolic network as a progression biomarker of premanifest Huntington's disease. J. Clin. Invest. 123, 4076–4088.
Tian, P., Teng, I.C., May, L.D., Kurz, R., Lu, K., Scadeng, M., Hillman, E.M., De Crespigny, A.J., D'Arceuil, H.E., Mandeville, J.B., Marota, J.J., Rosen, B.R., Liu, T.T., Boas, D.A., Buxton, R.B., Dale, A.M., Devor, A., 2010. Cortical depth-specific microvascular dilation underlies laminar differences in blood oxygenation level-dependent functional MRI signal. Proc. Natl. Acad. Sci. U. S. A. 107, 15246–15251.
Tong, Y., Yao, J.F., Chen, J.J., Frederick, B.D., 2018. The resting-state fMRI arterial signal predicts differential blood transit time through the brain. J. Cerebr. Blood Flow Metabol. 271678X17753329.
Uh, J., Lewis-Amezcua, K., Martin-Cook, K., Cheng, Y., Weiner, M., Diaz-Arrastia, R., Devous Sr., M., Shen, D., Lu, H., 2010. Cerebral blood volume in Alzheimer's disease and correlation with tissue structural integrity. Neurobiol. Aging 31, 2038–2046.
Uh, J., Lewis-Amezcua, K., Varghese, R., Lu, H., 2009. On the measurement of absolute cerebral blood volume (CBV) using vascular-space-occupancy (VASO) MRI. Magn. Reson. Med. 61, 659–667.
Uludag, K., Muller-Bierl, B., Ugurbil, K., 2009. An integrative model for neuronal activity-induced signal changes for gradient and spin echo functional imaging. Neuroimage 48, 150–165.
Uranova, N.A., Zimina, I.S., Vikhreva, O.V., Krukov, N.O., Rachmanova, V.I., Orlovskaya, D.D., 2010. Ultrastructural damage of capillaries in the neocortex in schizophrenia. World J. Biol. Psychiatr. 11, 567–578.
van Westen, D., Petersen, E.T., Wirestam, R., Siemund, R., Bloch, K.M., Stahlberg, F., Bjorkman-Burtscher, I.M., Knutsson, L., 2011. Correlation between arterial blood volume obtained by arterial spin labelling and cerebral blood volume in intracranial tumours. Magma 24, 211–223.
van Zijl, P.C., Eleff, S.M., Ulatowski, J.A., Oja, J.M., Ulug, A.M., Traystman, R.J., Kauppinen, R.A., 1998. Quantitative assessment of blood flow, blood volume and blood oxygenation effects in functional magnetic resonance imaging. Nat. Med. 4, 159–167.
Vazquez, A.L., Fukuda, M., Tasker, M.L., Masamoto, K., Kim, S.G., 2010. Changes in cerebral arterial, tissue and venous oxygenation with evoked neural stimulation: implications for hemoglobin-based functional neuroimaging. J. Cerebr. Blood Flow Metabol. 30, 428–439.
Vazquez, A.L., Lee, G.R., Hernandez-Garcia, L., Noll, D.C., 2006. Application of selective saturation to image the dynamics of arterial blood flow during brain activation using magnetic resonance imaging. Magn. Reson. Med. 55, 816–825.
Vis, J.C., Nicholson, L.F., Faull, R.L., Evans, W.H., Severs, N.J., Green, C.R., 1998. Connexin expression in Huntington's diseased human brain. Cell Biol. Int. 22, 837–847.
Warnert, E.A., Murphy, K., Hall, J.E., Wise, R.G., 2015. Noninvasive assessment of arterial compliance of human cerebral arteries with short inversion time arterial spin labeling. J. Cerebr. Blood Flow Metabol. 35, 461–468.
Watson, N.A., Beards, S.C., Altaf, N., Kassner, A., Jackson, A., 2000. The effect of hyperoxia on cerebral blood flow: a study in healthy volunteers using magnetic resonance phase-contrast angiography. Eur. J. Anaesthesiol. 17, 152–159.
Whittaker, J.R., Bright, M.G., Driver, I.D., Babic, A., Khot, S., Murphy, K., 2017. Changes in arterial cerebral blood volume during lower body negative pressure measured with MRI. Neuroimage. https://doi.org/10.1016/j.neuroimage.2017.1006.1041.
Williams, D.S., Detre, J.A., Leigh, J.S., Koretsky, A.P., 1992. Magnetic resonance imaging of perfusion using spin inversion of arterial water. Proc. Natl. Acad. Sci. U. S. A. 89, 212–216.
Wong, E.C., Cronin, M., Wu, W.C., Inglis, B., Frank, L.R., Liu, T.T., 2006. Velocity-selective arterial spin labeling. Magn. Reson. Med. 55, 1334–1341.
Wu, G., Luo, F., Li, Z., Zhao, X., Li, S.J., 2002. Transient relationships among BOLD, CBV, and CBF changes in rat brain as detected by functional MRI. Magn. Reson. Med. 48, 987–993.
Wu, Y., Agarwal, S., Jones, C.K., Webb, A.G., van Zijl, P.C., Hua, J., Pillai, J.J., 2016. Measurement of arteriolar blood volume in brain tumors using MRI without

exogenous contrast agent administration at 7T. J. Magn. Reson. Imag. 44, 1244–1255.
Xu, F., Liu, P., Pascual, J.M., Xiao, G., Lu, H., 2012. Effect of hypoxia and hyperoxia on cerebral blood flow, blood oxygenation, and oxidative metabolism. J. Cerebr. Blood Flow Metabol. 32, 1909–1918.
Yablonskiy, D.A., 1998. Quantitation of intrinsic magnetic susceptibility-related effects in a tissue matrix. Phantom study. Magn. Reson. Med. 39, 417–428.
Yablonskiy, D.A., Haacke, E.M., 1994. Theory of NMR signal behavior in magnetically inhomogeneous tissues: the static dephasing regime. Magn. Reson. Med. 32, 749–763.
Yablonskiy, D.A., Haacke, E.M., 1997. An MRI method for measuring T2 in the presence of static and RF magnetic field inhomogeneities. Magn. Reson. Med. 37, 872–876.
Yamori, Y., Horie, R., 1977. Developmental course of hypertension and regional cerebral blood flow in stroke-prone spontaneously hypertensive rats. Stroke 8, 456–461.
Yan, L., Li, C., Kilroy, E., Wehrli, F.W., Wang, D.J., 2012. Quantification of arterial cerebral blood volume using multiphase-balanced SSFP-based ASL. Magn. Reson. Med. 68, 130–139.
Ye, F.Q., Mattay, V.S., Jezzard, P., Frank, J.A., Weinberger, D.R., McLaughlin, A.C., 1997. Correction for vascular artifacts in cerebral blood flow values measured by using arterial spin tagging techniques. Magn. Reson. Med. 37, 226–235.
Zhao, J.M., Clingman, C.S., Narvainen, M.J., Kauppinen, R.A., van Zijl, P.C., 2007. Oxygenation and hematocrit dependence of transverse relaxation rates of blood at 3T. Magn. Reson. Med. 58, 592–597.
Zong, X., Kim, T., Kim, S.G., 2012. Contributions of dynamic venous blood volume versus oxygenation level changes to BOLD fMRI. Neuroimage 60, 2238–2246.